University of Kentucky Master's Theses   Graduate School

2008

MERGING OF FINGERPRINT SCANS OBTAINED FROM MULTIPLE CAMERAS IN 3D FINGERPRINT SCANNER SYSTEM

Deepthi Boyanapally
University of Kentucky, forudeepz@gmail.com

Right click to open a feedback form in a new tab to let us know how this document benefits you.

ABSTRACT OF THESIS

MERGING OF FINGERPRINT SCANS OBTAINED FROM MULTIPLE CAMERAS
IN 3D FINGERPRINT SCANNER SYSTEM

Fingerprints are the most accurate and widely used biometrics for human identification due to their uniqueness, rapid and easy means of acquisition. Contact based techniques of fingerprint acquisition like traditional ink and live scan methods are not user friendly, reduce capture area and cause deformation of fingerprint features. Also, improper skin conditions and worn friction ridges lead to poor quality fingerprints. A non-contact, high resolution, high speed scanning system has been developed to acquire a 3D scan of a finger using structured light illumination technique. The 3D scanner system consists of three cameras and a projector, with each camera producing a 3D scan of the finger. By merging the 3D scans obtained from the three cameras a nail to nail fingerprint scan is obtained. However, the scans from the cameras do not merge perfectly. The main objective of this thesis is to calibrate the system well such that 3D scans obtained from the three cameras merge or align automatically. This error in merging is reduced by compensating for radial distortion present in the projector of the scanner system. The error in merging after radial distortion correction is then measured using the projector coordinates of the scanner system.

KEYWORDS: Biometrics, Fingerprint Recognition, 3D Data Acquisition, Structured Light Illumination, Radial Distortion.

Deepthi Boyanapally

21st February, 2008

MERGING OF FINGERPRINT SCANS OBTAINED FROM MULTIPLE CAMERAS
IN A 3D FINGERPRINT SCANNER SYSTEM

By

Deepthi Boyanapally

Dr.Laurence G. Hassebrook
Director of Thesis

Dr.YuMing Zhang
Director of Graduate Studies

21st February, 2008
Date

RULES FOR THE USE OF THESIS

Unpublished thesis submitted for the Master's degree and deposited in the University of Kentucky Library are as a rule open for inspection, but are to be used only with due regard to the rights of the authors. Bibliographical references may be noted, but quotations or summaries are parts maybe published only with the permission of the author, and with the usual scholarly acknowledgements.

Extensive copying or publishing of the dissertation in whole or in part also requires the consent of the Dean of the Graduate school of the University of Kentucky.

A library that borrows this dissertation for use by its patrons is expected to secure the signature of each user.

Name   Date

_____
_____
_____
_____
_____
_____
_____
_____
_____
_____
_____
_____
_____
_____
_____
_____
_____
_____
_____
_____
_____
_____
_____

THESIS

DEEPTHI BOYANAPALLY

The Graduate School

University of Kentucky

2008

MERGING OF FINGERPRINT SCANS OBTAINED FROM MULTIPLE CAMERAS
IN A 3D FINGERPRINT SCANNER SYSTEM

THESIS

A thesis submitted in partial fulfillment of the
requirements for the degree of Master of Science in the
College of Engineering
at the University of Kentucky

By

Deepthi Boyanapally

Andhra Pradesh, India

Director: Dr. Laurence G. Hassebrook, Department of Electrical Engineering
Lexington, Kentucky

2008

DEDICATION

To my Family, Teachers and Friends

ACKNOWLEDGEMENTS

TABLE OF CONTENTS

LIST OF TABLES

LIST OF FIGURES

LIST OF FILES

CHAPTER ONE: INTRODUCTION

Biometrics is a science of recognizing an individual based on physical or behavioral traits. Some of the commonly used types of biometrics are fingerprints, palm prints, face, iris, retina etc. [1].

(a)	(b)	(c)	(d)
(e)	(f)	(g)	(h)
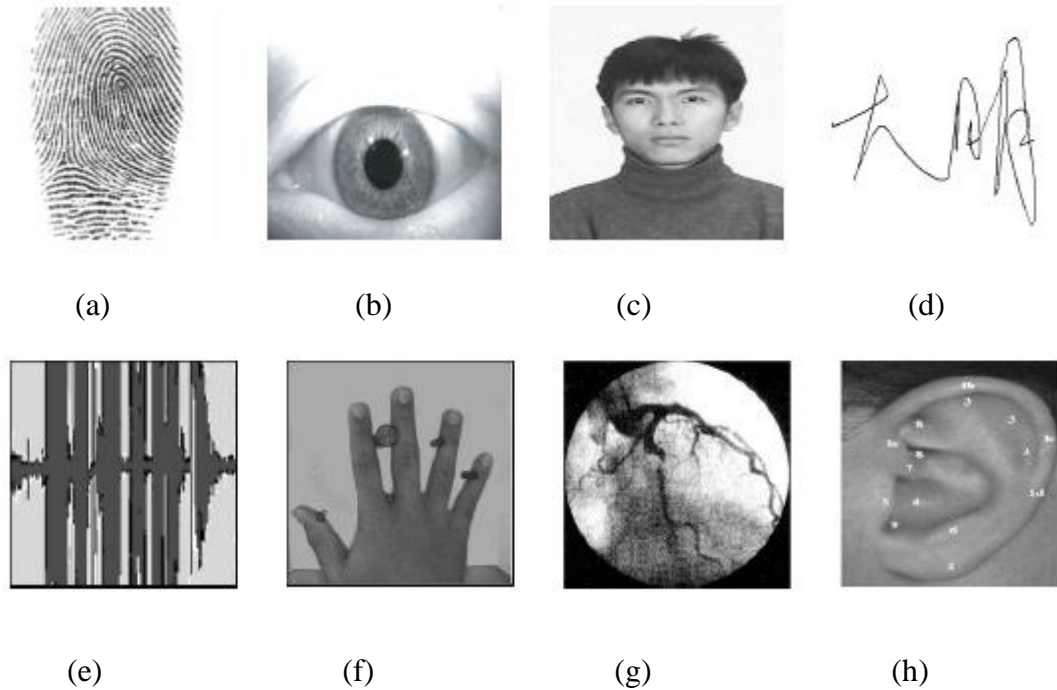
Fig. 1 Commonly used Biometrics[1]

The types of biometrics shown in the above figure 1 are:

(a) Fingerprint

(b) Iris

(c) Face Scan

(d) Signature

(e) Voice

(f) Hand Geometry

(g) Retina

(h) Ear

Fingerprint Identification Process

Fingerprints are the most accurate and widely used biometrics due to their uniqueness, rapid acquisition and easy means of acquisition. Fingerprints have been in use for human identification since late nineteenth century. Due to the overwhelming demand for fingerprint recognition which required many man hours for the manual process, efforts were made to automate the fingerprint identification process. This led to the development of an Automatic Fingerprint Identification System (AFIS) [3].
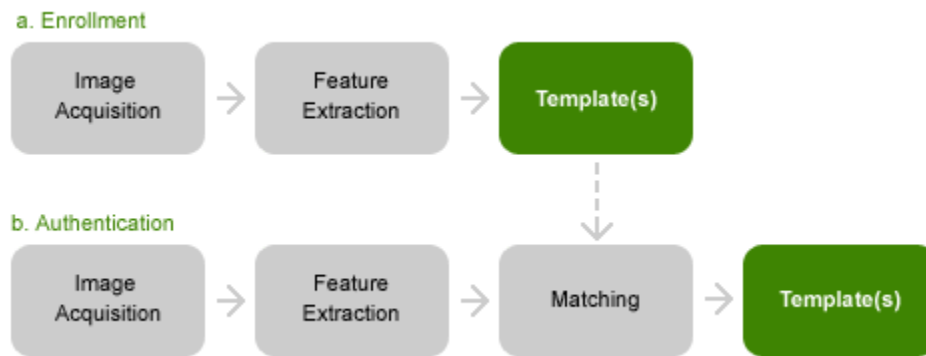
Fig. 2 Fingerprint Identification Process [2]

Fingerprint Acquisition

Fingerprint acquisition can be classified into off-line and live scan techniques. One of the common offline techniques is the ink technique where finger is spread with ink and pressed against a paper. The paper is scanned to produce a digital image. Excessive inking or deficit ink produces bad quality fingerprint images. In live scan techniques, the finger is pressed against the surface of the scanner which is sensed by a sensor producing a digital fingerprint image. The live scan technique is user friendly, reliable and low cost which also makes it useful for civil and commercial applications apart from benefiting AFIS. The advantage of using offline scanning technique is that it produces a rolled equivalent whereas the live scan technique requires a skilled technician to roll the finger in a synchronized manner with the live scan. For identification, live scan uses a flat impression which is produced by pressing finger against the surface of the scanner [4].

2

In a live scan technique scanner system, the sensor that produces the fingerprint image is the most important part. Based on the type of sensor used, live scan techniques can be classified as optical, solid state and ultrasound. In optical sensors, we have Frustrated Total Internal Reflection (FTIR) live scan technique, optical fiber sensors, electro-optical and direct reading techniques. The solid state sensors can be divided into capacitive, thermal, electric field and piezoelectric sensors [4].

Fingerprint Features

A fingerprint appears as a pattern of interleaved ridges and valleys where ridges are dark lines and valleys are bright in color. The width of ridges varies from $100\,\mu m$ to $300\,\mu m$ [4]. Fingerprint information is divided into three levels for identification purposes. Level 1 features are ridge patterns which are used for classification of fingerprints as shown in Figure 3. Level 2 features are minutia shown in Figure 4. Minutia refers to various ways the ridges in a fingerprint can be discontinuous. Minutiae are the most reliable features used for fingerprint identification. Level 3 features are pores and ridge shape shown in Figure 5 [5].

| Arch (A) | Tented Arch (T) | Whorl (W) | Loop (U or R) |
| (a) | (b) | (c) | (d) |
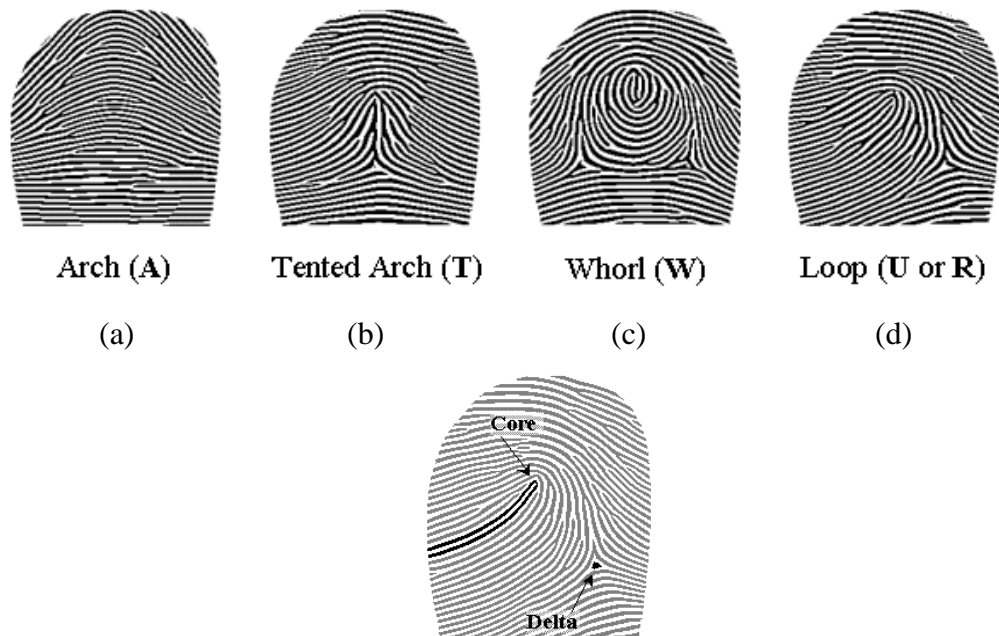
Fig. 3 Level 1 Features - Ridge Patterns [6]

.
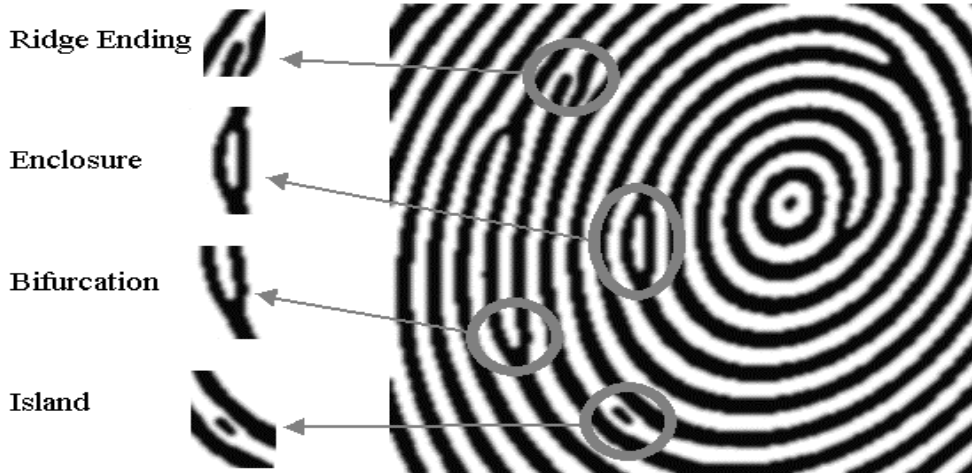
Fig. 4 Level 2 features – Minutia [6]

PORES   LINE SHAPE   INCIPIENT RIDGES
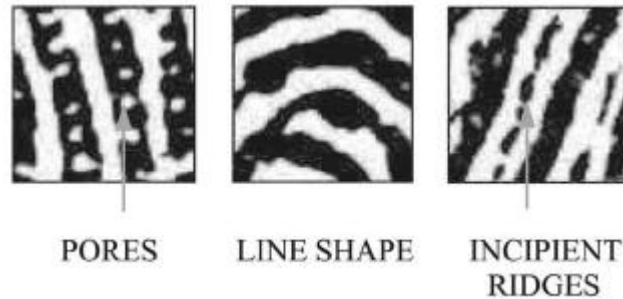
Fig. 5 Level 3 features – Pores, Ridge Shapes [5]

Fingerprint Matching

Fingerprint Matching is a method of comparing two fingerprint images and finding the similarities between them. A large number of algorithms have been developed to achieve matching and the choice of a matching algorithm depends on the representation of the fingerprint image. These fingerprint matching algorithms can be classified as correlation based technique, minutiae based technique and ridge feature based matching. These matching techniques were tested on various databases to determine which algorithm is the best. It was found that minutiae based algorithms performed better when compared to correlation based algorithms. However, for poor quality fingerprint images, minutiae cannot be extracted well and correlation based matching has to be used [7].

NIST conducted studies on fingerprint matching using a huge database of fingerprints obtained from various sources and with varying image quality. The studies were

4

conducted using a fingerprint matcher called the verification test bed (VTB) which can be used as the reference for other fingerprint matchers. These studies compare the fingerprints obtained from various sources, determine the quality of fingerprint images obtained from ink and live scan techniques and find the accuracy of matching plain (flat) to rolled fingerprint images. Results show that the accuracy of rolled to rolled matching is much higher than plain (flat) to plain (flat) and plain(flat) to rolled matching [8]. Several other studies on matching performance of a system using flat fingerprints [9] and plain (flat) to rolled matching using algorithmic test bed (ATB) [10] were conducted by NIST. These studies serve as a reference for evaluating the performance of a large number of fingerprint identification systems developed over the past few years. NIST evaluated the performance of fingerprint matching algorithms obtained from different vendors. These experiments were conducted on a large set of fingerprint databases [11]. Zin Chu Wu et.al., proposed a non-parametric method to analyze the distribution functions of match and non- match similarity scores of a large scale database which helps in evaluating the performance of fingerprint matching algorithms.   A non parametric method is implemented since the match and non match similarity scores do not have any specific distribution function. In this method, the area under receiver operating characteristics curve (ROC) is used to evaluate the performance of matching algorithms. This area when computed using the trapezoidal rule gives the Mann-Whitney statistic which is directly formed from the match and non match similarity scores. This statistic can then be used to find the significance of the difference in area of two ROC curves and hence helps in evaluating the performance of fingerprint matching from different vendors [12]. The size of fingerprint databases used by NIST for evaluating fingerprint data and matching software is huge. It is necessary that the dataset size be reduced to an optimum value which will obtain efficiency and accuracy in evaluating the fingerprint data. Zin Chu Wu et.al., presents a method to calculate the optimum sample size of the biometric data required to evaluate fingerprint data using the Chebyshev's inequality and random sampling [13].

Efforts are being made to develop non contact 3D fingerprint scanners that produce rolled equivalent fingerprints. A multi camera touch less device has been developed in which

five cameras are placed surrounding the finger and a series of 16 images of the same portion of the finger are captured by each camera. Using these images at different illumination conditions, the special features of the image are extracted. Using the principles of stereo vision and photogrammetry the 3D reconstruction is done [14]. The 3D fingerprint images obtained cannot be directly used for identification purposes since the Automated Fingerprint Identification System (AFIS) consists of legacy rolled images. The main challenge in using 3D fingerprint scanners is the compatibility between the 3D fingerprint images and the legacy rolled images. Yi Chen et.al., present a non parametric unwrapping algorithm that unfolds the 3D fingerprint as if the 3D finger was rolled onto a 2D plane. There are two types of unwrapping methods: Parametric and Non-parametric. In parametric unwrapping the 3D object is projected onto a parametric model like a cylinder or sphere. However, these methods introduce a large number of distortions while unwrapping. In non-parametric unwrapping, efforts are made to preserve the local distances and angular relations and no parametric models are used. The results obtained by this algorithm are compared with its rolled image [14].

Motivation

Both offline and live scan techniques of fingerprint acquisition have several disadvantages. These techniques are contact based which can lead to deformation of fingerprint features and reduced capture area. Improper skin conditions, worn finger ridges, bad acquisition conditions can result in poor quality fingerprints. Also, the process is very slow, not user friendly and requires the supervision of a technician to capture the fingerprint images. This has resulted in increased demand for a high speed, non-contact and accurate fingerprint acquisition technique.

Thesis Overview

A high resolution, high speed, non-contact 3D surface scanning system has been developed to acquire a 3D scan of a finger using structured light illumination technique. The 3-D data is unwrapped into two dimensional fingerprints. The scanner system consists of an array of three cameras, projector and a scan volume for the finger to be scanned. A single camera cannot capture the 3D scan of the finger from one end of the nail to the other end. So three cameras separated by 45 degree angles are used in the

scanner system. Each camera produces a 3D scan of the finger. By merging the 3D scans obtained from the three cameras a nail to nail fingerprint scan is obtained. Nail to nail scans help in acquiring more fingerprint information useful for the recognition process and also produces an unraveled image similar to the ink method where the finger is rolled on a paper from one end of the nail to nail to the other end. However, the scans from the cameras do not merge properly.

The main objective of this thesis is to calibrate the system well such that the 3D scans obtained from the three cameras merge or align automatically. The accuracy of merging can be improved by compensating for distortions present in the camera and projector of the scanner system. These distortions which are caused due to lens aberrations are Radial Distortion, Perspective Distortion and Gamma Correction. The most significant distortion present in wide angle lenses or lenses of short focal length is Radial Distortion.

Radial Distortion causes the image coordinates to be distorted in the radial direction. The cameras and projector of scanner system are tested for the presence of radial distortion. The projector showed significant radial distortion. The projector optical center and radial distortion coefficients are calculated and the radial distortion in the projector space is corrected. After the correction of radial distortion the scanner system is calibrated and the merged 3D scans from the cameras are observed. A significant improvement in merging is observed after the radial distortion correction. Merged scans of different objects before and after radial distortion correction are compared. The radial distortion correction of projector in the fingerprint scanner system reduces the error in merging to some extent but did not eliminate it completely. This error in merged scan is determined by finding the distance between world coordinates of corresponding points from the three cameras. The corresponding points between the three different cameras in a structured light system can be found based on the concept of projector space. The projector space for all the cameras in the scanner system is the same. Hence, ideally for a point in the 3D world coordinate system captured by the three cameras, the projector coordinates of this point for all the three cameras should remain the same. Using this constraint, the corresponding points in the three cameras can be determined and the distance between these points is

calculated. Finally, the merged 3D scans are unraveled to 2D images using a software program (developed by Yongchang Wang, Center for Visualisation and Virtual Environment, University of Kentucky).

Thesis Organization

This thesis is divided into five chapters. Chapter 1 gives an introduction and overview on the fingerprint identification process and 3D fingerprint techniques developed so far and overview of the thesis. Chapter 2 gives an introduction to the concept of structured light illumination and the existing structured light illumination methods. We then proceed to describe the process of Calibration which is the first step in 3D data acquisition. Linear and two step calibration techniques which take distortion models into account are discussed in detail. This is followed by an introduction to various types of distortions present in lenses. Radial and Perspective distortion correction methods which are implemented in our fingerprint scanner system are explained in detail.

In chapter 3, the problem of Merging in our 3D fingerprint scanner system is discussed. The concept of Radial Distortion is introduced and the distortion correction methodology which increases the accuracy of merging is explained in detail.

In chapter 4, the error in the calibrated data is analyzed and the error in the merged scans is determined by using the projector coordinates or phase information. Chapter 5 discusses the experimental results obtained from the radial distortion correction, accuracy of merged scans and 2D unraveled images of the merged scans. Chapter 6 discusses the conclusions made from the thesis work and future research work.

CHAPTER TWO: BACKGROUND

In the first section of this chapter, the concept of structured light illumination for 3D Data Acquisition is explained. The second section in this chapter deals with the various calibration techniques that can be used for structured light scanner systems. The third section explains the various optical distortions caused due to lens aberrations. Radial and Perspective Distortions, which are a common phenomena in structured light systems, are explained in detail in the following section.

Research studies in the field of 3D data acquisition have become increasingly popular over the past few years because of its diverse applications. Jarvis presents a good survey on the development of various range finding methods over the years [16]. Blais presents a review of the development of various range sensor systems during the past 20 years [17].

Time of Flight Systems [18], Structured Light Method [19], Moire Fringe Method [20], Stereo Vision [21] are some of the commonly used 3D data acquisition techniques.

Stereovision is one of the most popular and widely used techniques of 3D data acquisition. But the problem of correspondence between cameras limited the use of stereovision. The correspondence problem was solved by Structured Light Illumination technique [22].

Structured Light Illumination

A Structured Light Illumination System consists of an array of cameras, a projection unit and a scan volume. Light patterns of multiple frequencies are projected onto an object and the three dimensional depth of the object is reconstructed from the distortions in the reflected and captured images. The depth reconstruction is based on the concept of Optical Triangulation. A basic structured light system consisting of a camera, projector and the object to be scanned along with the camera, projector and world coordinate system as represented in Figure 6.
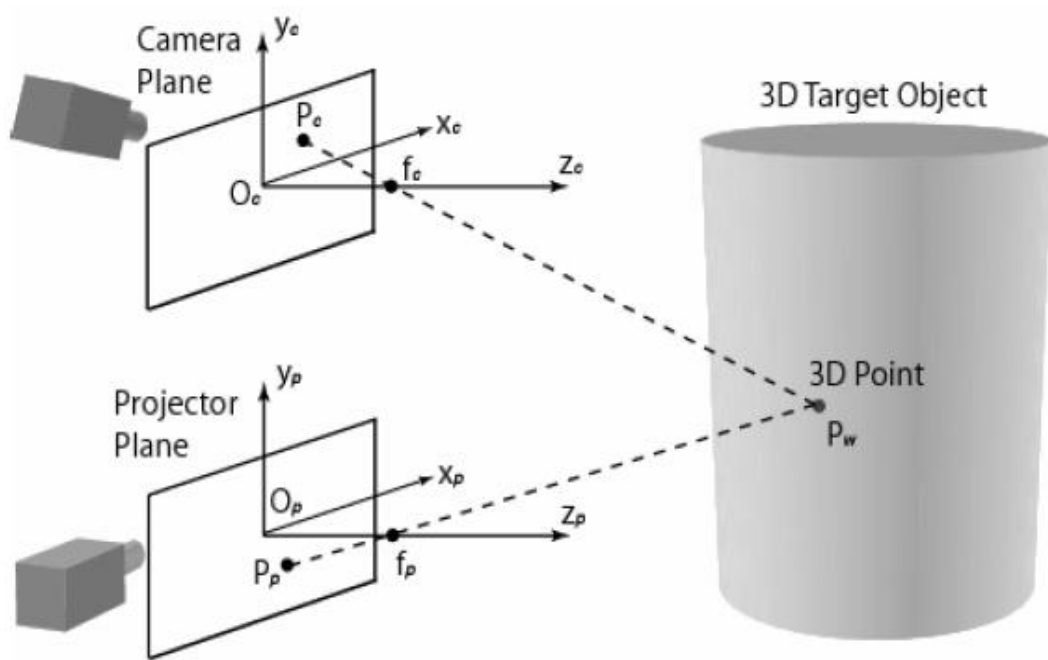
Fig. 6 Basic Structured Light System [23]

In traditional structured light illumination methods, a single light stripe is used to scan the entire surface of the object and this method requires that the object maintain its position still during the entire scanning period [19]. Will et al. [24] recommended the use of a grid coded light pattern that illuminates the entire object surface at once as this reduces the burden of processing each scan.

Another technique, multiple light stripe patterns also requires the entire object surface to be illuminated at once. However, these patterns result in ambiguities and a lower lateral resolution. The ambiguity problem is solved by encoding the surface with multiple light patterns of varying frequencies. The lateral resolution is improved by optimizing the encoded spatial frequency [25].

Hassebrook et al. [19] has introduced a method where multiple light patterns are combined into a single composite pattern by spatially modulating them along the orthogonal direction that is perpendicular to the phase dimension. The concept of Phase Measuring Profilometry for multiple patterns is utlilized here.

The Multi-frequency Phase Measuring Profilometry (PMP) increases the quality of the scan by using both high and low frequency light patterns. The high frequency increases the accuracy of depth measurement but produces ambiguity errors. Hence a low frequency pattern is used to unwrap the high frequency pattern for reconstruction of non ambiguous depth [26].

Calibration

The foremost step in the process of 3D data acquisition using structured light illumination technique is Calibration. Camera Calibration establishes a relation between world coordinates and camera coordinates of a system by determining the intrinsic and extrinsic parameters of the camera. The intrinsic parameters determine the physical and optical characteristics of the camera and the extrinsic parameters determine the position and orientation of the camera with respect to the world coordinate system [27].

Salvi et al. [27] gives a detailed description of popular calibration techniques for 3D data acquisition. Linear calibration technique uses least square method or singular value decomposition to obtain the camera parameters. Even though this technique is simple and fast to compute, lens distortions are not taken into account. Non linear calibration techniques take lens distortion models into account but they require many iterations to determine the parameters. In two step techniques, the first step solves for the calibration parameter using linear methods and second step involves non linear optimization of these parameters taking distortion models into account.

Some of the linear and two step techniques are detailed here:

Faugeras, Toscani [1986] proposed a calibration technique in which, given the world and image coordinates of the reference points, the camera transformation matrix can be determined by using the linear least square solutions method. This model is simple and fast to compute since it is linear. However, this method does not take lens distortions into consideration.

Weng et al. [29] proposed a two step method of camera calibration which takes radial, decentering and thin prism distortions into account. The first step involves a closed form solution to compute the parameters of the camera and does not take distortion models into account. The second step is a non linear optimization problem that takes distortions into account and uses the solution from the first step as its initial value. This two step approach has the advantage of increasing the accuracy since the initial guess obtained from a closed form solution serves as a good starting value. Tsai[30] and Wei et al.[31] have also presented two step calibration techniques taking the distortion models into account.

Zhang [32] presents a new method of Camera Calibration which is highly flexible, low cost and robust. Images of a planar pattern captured by the camera in at least two different orientations is required to determine the internal and external parameters of the camera. A closed form solution involving singular value decomposition is used to find the internal and external parameters of the camera. A non linear refinement of the camera parameters based on the maximum likelihood criterion is done by using the Levenberg-Marquardt Algorithm. Lens distortions like radial distortion are considered while using non linear refinement.

Distortions in Camera
Lens distortions are a consequence of laws of refraction associated with spherical surfaces. Careful design of lens will minimize the aberrations. Lenses exhibit various kinds of aberrations like coma, spherical, astigmatism, field curvature and radial distortion.

The aberration is given by

$$a(Q) = C_1 r^4 + C_2 h r^3 \cos\theta + C_3 h^2 r^2 \cos^2\theta + C_4 h^2 r^2 + C_5 h^3 r \cos\theta \qquad (2.1) [33]$$

where Q is the optical axis, $a(Q)$ is the aberration at Q, r is the aperture of the refracting surface, θ is the symmetry around the optical axis, h is the departure from axial imaging,

and C_i for $i=$ 1 to 5 are constant parameters of the model. Each component of the equation represents an aberration and is given in Table 2.1. [33]

Table 1 Seidal Aberrations [33]

Components	Aberration
r^4	Spherical Aberration
$hr^3 \cos\theta$	Coma
$h^2 r^2 \cos^2\theta$	Astigmatism
$h^2 r^2$	Curvature of Field
$h^3 r \cos\theta$	Distortion

Spherical Aberration

Spherical aberration is caused by the curvature of a spherical lens [33]. The rays parallel to the principal axis, and incident on the outer edges of the lens do not focus at the same point as the other rays. This results in blurry images and is called Spherical aberration.

.
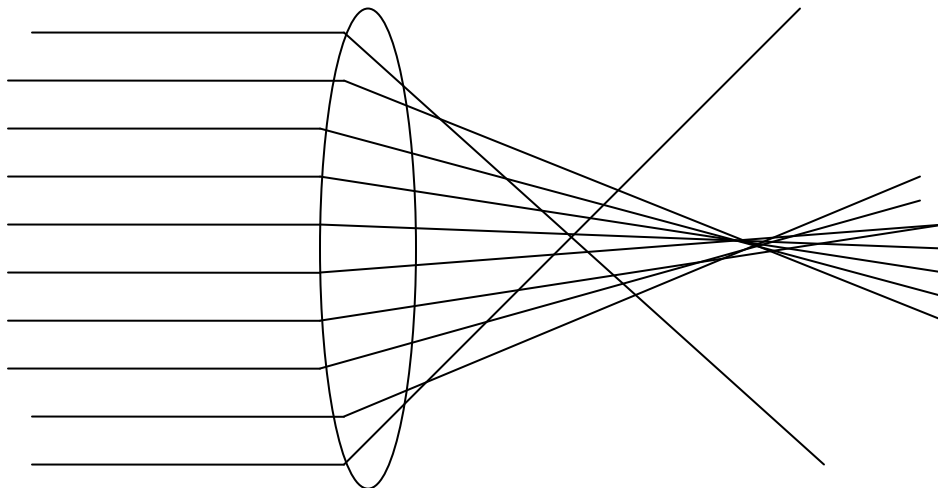
Fig. 7 Spherical Aberration in lens

13

Comatic Aberration

Comatic aberration is variation of the magnification and focus as a function of the radial distance to the optical axis. As the object is moved away from the optical axis, the aberration appears as a flaring of the point similar to the tail of a comet [33].

Astigmatism and Field of Curvature Aberrations

Astigmatism results in different foci in the vertical and horizontal tangential planes. Field of curvature distortion results due to the curvature of the lens system producing a curved image of a flat object [33].

Radial Distortion

Radial Distortions mostly occur in wide angle lenses. Radial distortions distort the image points only in the radial direction. For wide angle lenses, the points move towards the optical center along the radial direction called Barrel Distortion shown in Figure 8(a). When the points move further away from the optical center Pincushion Distortion occurs shown in Figure 8(b) [35].
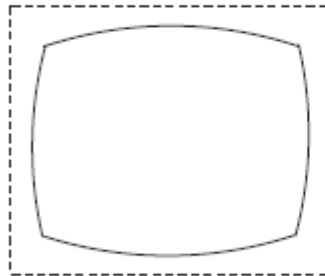
(a) Barrel Distortion [35]
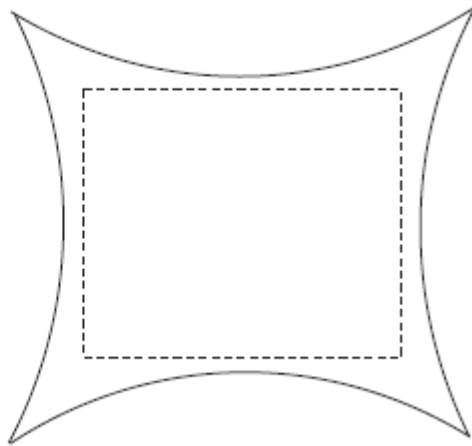
(b) Pincushion Distortion [35]

Fig. 8 Types of Radial Distortion

Most of the radial distortion correction methods make use of a polynomial radial distortion model given by

$$r_2 = r_1 + \alpha r_1^3 + \beta r_1^5 + ... \qquad (2.2)\ [33]$$

where r_1 is the distorted radius and r_2 is the undistorted radius.

Over the past few years, various techniques were developed to resolve the problem of radial distortion. Some of the prominent works are described in the below paragraphs.

Tsai [30] and Weng et al. [29], resolved the radial distortion by using a calibration object with known 3D world coordinates. A two step camera calibration technique which takes lens distortions into consideration is presented by them. The first step is a closed form solution giving the camera parameters in a distortion free model. Second step does non linear optimization taking distortion into consideration with initial value from the first step. These two step techniques give accurate results because the initial guess obtained from a closed form solution serves as a good starting value.

Rahul Swaminathan et al. [34] and Thorsten et al. [39] implemented radial distortion correction based on the concept that straight lines in the 3D world have to appear as

straight lines in the images. Thorsten et al. [39] uses a non linear inverse radial distortion model to correct the distortion.

A new method for modeling radial distortion based on the camera and the lens projective geometry is proposed. It is assumed that distortion is not an error of lens design. This model is dependent on the focal length of the lens and does not introduce any distortion specific parameters. However, very few experimental results are provided to support the concept [35].

Richard Hartley et al. [36] proposed a method for radial distortion correction while calibrating the internal calibration parameters. This method requires the use of a planar calibration pattern and the distortion correction is an add-on to Zhang [32] method of calibration. The advantage of this method is that it does not use any radial distortion model and hence applicable to a large number of cameras. The correction process is also non iterative and hence there are no convergence problems.

Ma et al. [37] proposed a piecewise radial distortion model for radial correction. This technique uses analytical piecewise model in order to increase the flexibility of the system and analytically solve the distortion problem.

De et al. [38] presents a method which is applied to cameras with large lens distortions. An iterative technique performs distortion correction with subsequent calculation of internal and external parameters of camera. This technique is very useful because a majority of other techniques first determine the calibration parameters and then correct for distortion which could lead to inaccuracy in calibration for cameras with large lens distortions.

Hassebrook et al. [33] have presented techniques for correcting Radial and Perspective Distortions. Radial Distortion is corrected digitally using a look up table (LUT) which is created by calibrating with a grid pattern.

Perspective Distortion

Perspective projection is the mapping of the 3D world coordinates onto a 2D image plane. The concept of perspective projection in a pin hole camera model is shown in Figure 9.
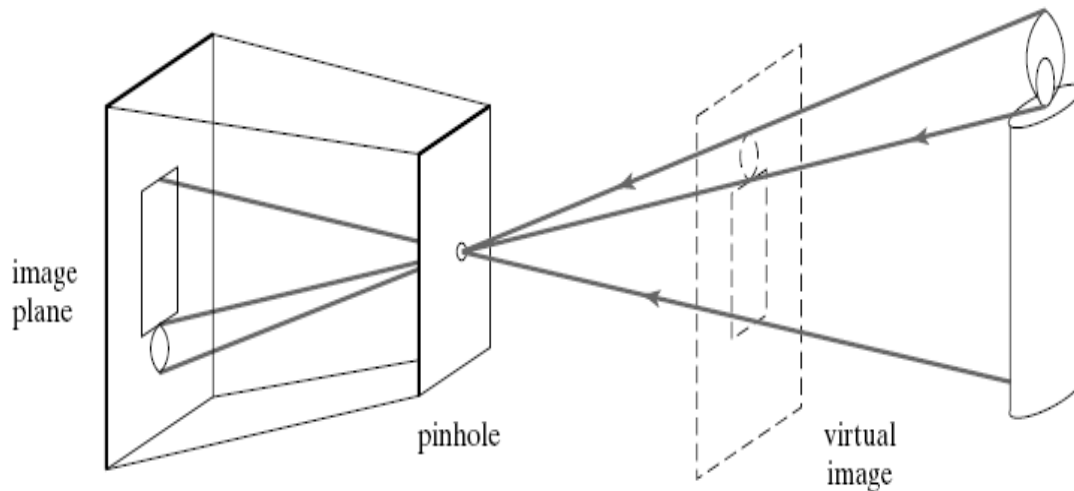
Fig. 9 Pin Hole Camera Model [40]

Rays of light from the object enter through the small pin-hole aperture of the camera and intersect the image plane to form the image. The image produced is inverted and a virtual image is obtained by placing the image plane in front of the camera at an equal distance. Some of the effects of Perspective Projection are the size of the image is inversely proportional to its distance and the images of parallel lines on further extension intersect at a point called vanishing point [40].

The effects caused by perspective projection lead to Perspective Distortion. Figure 10 shows a rectangular grid with perspective distortion.
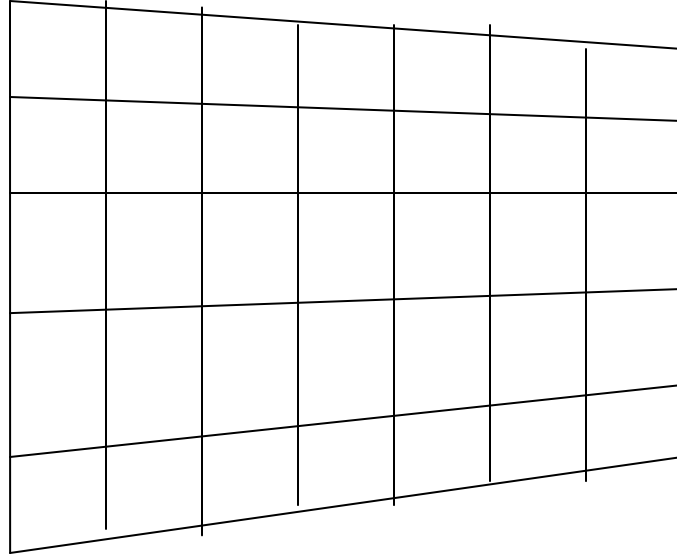
Fig. 10 Rectangular grid with perspective distortion[33]

Hassebrook et al. [33] presented various methods like the use of telecentric lenses and digital processing to decrease perspective distortion. The digital distortion reduction is application dependent. In applications such as scanning of a printed surface for optical character recognition systems the text is imaged from non normal angle and perspective correction is done using SVD technique of Tsai [30]. For stereo vision applications, correction is based on the principle that a single world coordinate defines intersecting rays from two cameras. Another application is in pattern recognition where distortion invariant correlation filtering is used to detect location of target independent of distortion.

CHAPTER THREE: MERGING OF FINGERPRINT SCANS

In 3D Fingerprint Scanner System, one camera cannot capture the finger image from one end of the nail to the other end. Multiple cameras placed at different angles with respect to the finger yield multiple 3D scans of the finger. Merging of 3D scans obtained from different angles produces a nail to nail fingerprint scan. In this system, three cameras separated by 45 degree angles are utilized to obtain nail to nail scans. The accuracy of merging scans from different cameras can be improved by compensating for distortions due to lens aberrations in the camera and the projector. The most significant distortions present in lenses are Radial Distortion and Perspective Distortion.

The goal of this research work is to calibrate the system accurately by compensating for the various lens distortions so that the scans from different cameras align automatically.
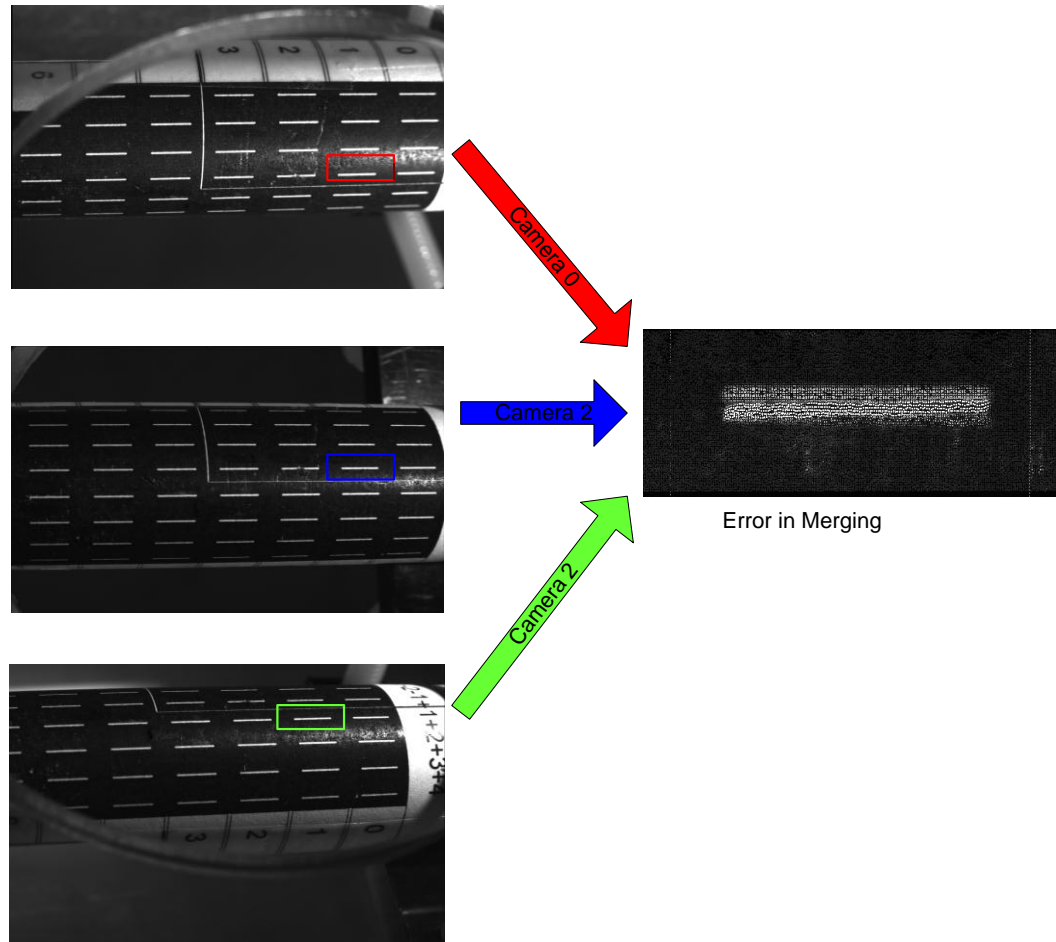
Fig. 11 Merging of Scans from three Cameras

Multi Camera 3D Fingerprint Scanner System

A Structured Light 3D Fingerprint scanner system consists of an array of cameras, a projector and a scan volume for the placement of the object to be scanned. A background pattern with predetermined world coordinates is used to calibrate the system. Light patterns of multiple frequencies are projected onto the object to be scanned and the three dimensional range of the object is calculated from the distortions in the reflected and captured image. Each camera captures a portion of the object and all the captured images are merged together based on the predetermined world coordinates of the background pattern to produce a super image. Figure 12 shows a block diagram of the Multi camera Fingerprint Scanner System.
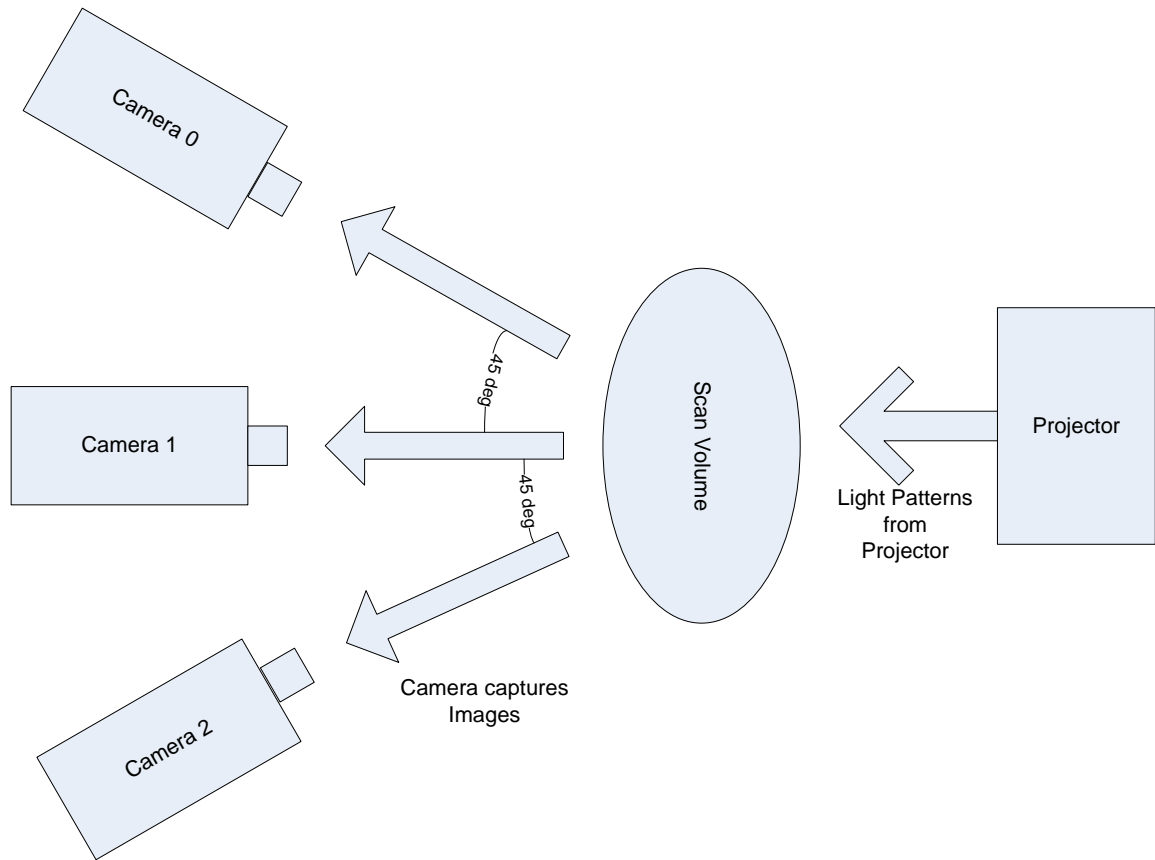
Fig. 12 Multi-camera Fingerprint Scanner System

Experimental Setup

The system consists of a Mitsubishi PK 10 DLP projector, three Pulnix cameras and a scan volume.

Calibration of Fingerprint Scanner System

The grid used to calibrate the system is shown in Figure 13. The world coordinates of the center of the white lines are predetermined.
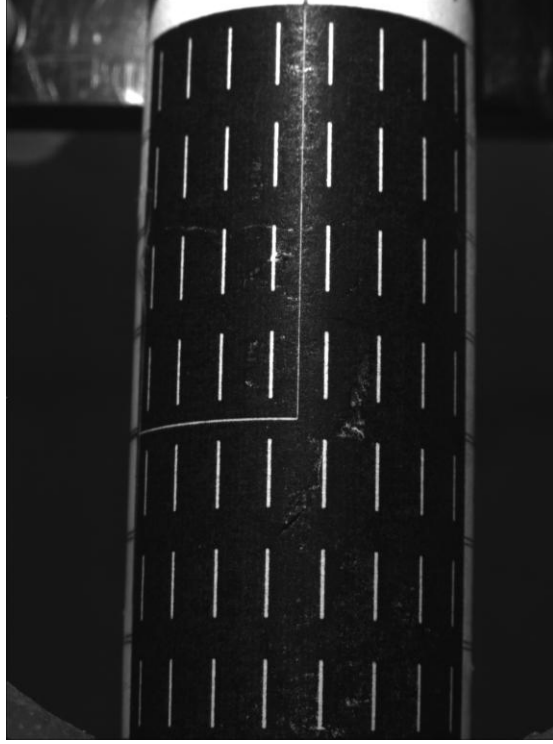
Fig. 13 Calibration Grid

Calibration software determines the camera coordinates (x^c, y^c) and projector coordinates (x^p, y^p) for the corresponding world coordinates (X^w, Y^w, Z^w). The calibration parameters M^{wc}, M^{wp} are calculated using the Least squares solution technique.

Least Squares Solution Method: The transformation from world to camera coordinate system is given by [26]

$$x^c = \frac{m_{11}^{wc} X^w + m_{12}^{wc} Y^w + m_{13}^{wc} Z^w + m_{14}^{wc}}{m_{31}^{wc} X^w + m_{32}^{wc} Y^w + m_{33}^{wc} Z^w + m_{34}^{wc}} \tag{3.1}$$

$$y^c = \frac{m_{21}^{wc} X^w + m_{22}^{wc} Y^w + m_{23}^{wc} Z^w + m_{24}^{wc}}{m_{31}^{wc} X^w + m_{32}^{wc} Y^w + m_{33}^{wc} Z^w + m_{34}^{wc}} \tag{3.2}$$

The camera transformation matrix is

$$M^{wc} = \begin{bmatrix} m_{11}^{wc} & m_{12}^{wc} & m_{13}^{wc} & m_{14}^{wc} \\ m_{21}^{wc} & m_{22}^{wc} & m_{23}^{wc} & m_{24}^{wc} \\ m_{31}^{wc} & m_{32}^{wc} & m_{33}^{wc} & m_{34}^{wc} \end{bmatrix} \qquad (3.3)$$

The transformation from world to projector coordinates is given by [12]

$$x^p = \frac{m_{11}^{wp} X^w + m_{12}^{wp} Y^w + m_{13}^{wp} Z^w + m_{14}^{wp}}{m_{31}^{wp} X^w + m_{32}^{wp} Y^w + m_{33}^{wp} Z^w + m_{34}^{wp}} \qquad (3.4)$$

$$y^p = \frac{m_{21}^{wp} X^w + m_{22}^{wp} Y^w + m_{23}^{wp} Z^w + m_{24}^{wp}}{m_{31}^{wp} X^w + m_{32}^{wp} Y^w + m_{33}^{wp} Z^w + m_{34}^{wp}} \qquad (3.5)$$

The projector transformation matrix is

$$M^{wp} = \begin{bmatrix} m_{11}^{wp} & m_{12}^{wp} & m_{13}^{wp} & m_{14}^{wp} \\ m_{21}^{wp} & m_{22}^{wp} & m_{23}^{wp} & m_{24}^{wp} \\ m_{31}^{wp} & m_{32}^{wp} & m_{33}^{wp} & m_{34}^{wp} \end{bmatrix} \qquad (3.6)$$

The parameters m_{34}^{wc} and m_{34}^{wp} are assumed to be 1. The parameter matrices can be written in vector form as [26]

$$m_c = \begin{bmatrix} m_{11}^{wc} & m_{12}^{wc} & m_{13}^{wc} & m_{14}^{wc} \dots m_{34}^{wc} \end{bmatrix} \qquad (3.7)$$

$$m_p = \begin{bmatrix} m_{11}^{wp} & m_{12}^{wp} & m_{13}^{wp} & m_{14}^{wp} \dots m_{34}^{wp} \end{bmatrix} \qquad (3.8)$$

The solution to equation $Am_c = B$ gives the camera parameters, where A is given by [12]

$$A_{2i-1} = \begin{bmatrix} X_i^w \\ Y_i^w \\ Z_i^w \\ 1 \\ 0 \\ 0 \\ 0 \\ 0 \\ -x_i^c X_i^w \\ -x_i^c Y_i^w \\ -x_i^c Z_i^w \end{bmatrix}^T \qquad A_{2i} = \begin{bmatrix} 0 \\ 0 \\ 0 \\ 0 \\ X_i^w \\ Y_i^w \\ Z_i^w \\ 1 \\ -y_i^c X_i^w \\ -y_i^c Y_i^w \\ -y_i^c Z_i^w \end{bmatrix} \qquad (3.9)$$

and *B* is given by

$$B_{2i-1} = \begin{bmatrix} x_i^c \end{bmatrix} \qquad\qquad B_{2i} = \begin{bmatrix} y_i^c \end{bmatrix} \qquad (3.10)$$

The least squares solution is given by [26]

$$m_c = \left(A^T A\right)^{-1} A^T B \qquad (3.11)$$

The projector transformation matrix is calculated in a similar way.

Using the transformation matrices of the camera and the projector, camera coordinates (x^c, y^c) and projector coordinate y^p, 3D world coordinates of the object are reconstructed.

Equations for the reconstruction of 3D world coordinates are given by [12]

$$C = \begin{bmatrix} m_{11}^{wc} - m_{31}^{wc} x^c & m_{12}^{wc} - m_{32}^{wc} x^c & m_{13}^{wc} - m_{33}^{wc} x^c \\ m_{21}^{wc} - m_{31}^{wc} y^c & m_{22}^{wc} - m_{32}^{wc} y^c & m_{23}^{wc} - m_{33}^{wc} y^c \\ m_{21}^{wp} - m_{31}^{wp} y^p & m_{22}^{wp} - m_{32}^{wp} y^p & m_{23}^{wp} - m_{33}^{wp} y^p \end{bmatrix} \qquad (3.12)$$

$$D = \begin{bmatrix} m_{34}^{wc} x^c - m_{14}^{wc} \\ m_{34}^{wc} y^c - m_{24}^{wc} \\ m_{34}^{wp} y^p - m_{24}^{wp} \end{bmatrix} \qquad (3.13)$$

$$P = \begin{bmatrix} X^w & Y^w & Z^w \end{bmatrix}^T = C^{-1} D \qquad (3.14)$$

Radial Distortion

Radial distortion is one of the most significant distortions present in wide angle lenses. This distortion is caused due to imperfect lenses. In radial distortion, points in the image plane are distorted in the radial direction. Deviations are most noticeable for rays that pass through the edge of the lenses.

The two common types of radial distortions are barrel distortion and pin cushion distortion. In barrel distortion, the points move closer towards the optical center and in pin cushion distortion the points move away from the optical center. Barrel distortion is more prominent in wide angle or lenses with short focal length.
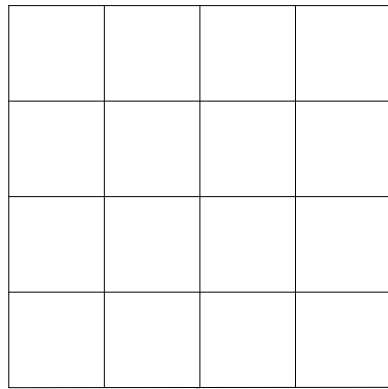
(a) Undistorted Grid
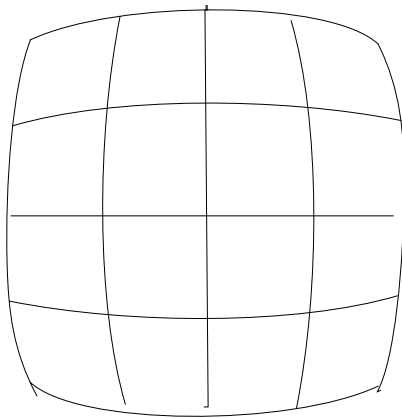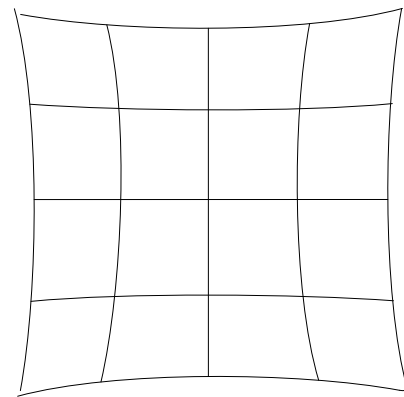
(b) Barrel Distortion   (c) Pincushion Distortion

Fig. 14 Radial Distortion

25

The general mathematical model used to implement radial distortion correction is

$$r_2 = r_1 + \alpha r_1^3 + \beta r_1^5 + ... \tag{3.15}$$

where r_1 is the distorted radius, r_2 is the undistorted or corrected radius and α, β are the distortion coefficients.

The polynomial equation (3.15) can be reduced to consist of only terms which are most significant for distortion correction, as shown in equation (3.16).

$$r_2 = r_1 + \alpha r_1^3 \tag{3.16}$$

Presence of Radial Distortion

To detect the presence of radial distortion in the cameras, images of a grid pattern placed on a flat surface in the scan volume are captured by the three cameras as shown in figures 15, 16 and 17. It is observed from the captured images that there is no significant radial distortion present in the cameras of the scanner system.

Fig. 15 Camera 0 capture of the Grid Pattern
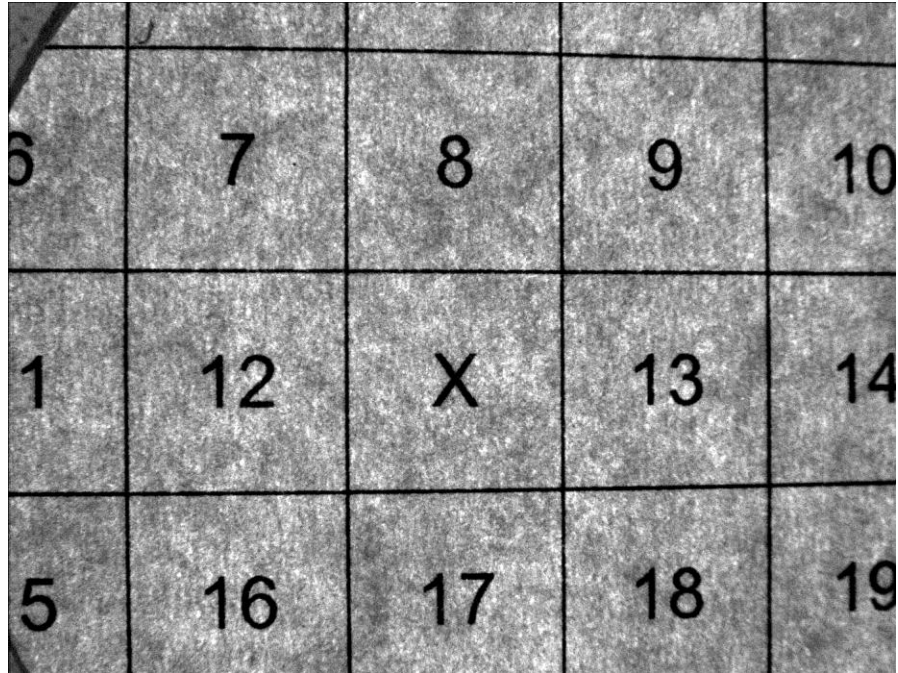
Fig. 16 Camera 1 capture of the Grid Pattern (Center Camera)
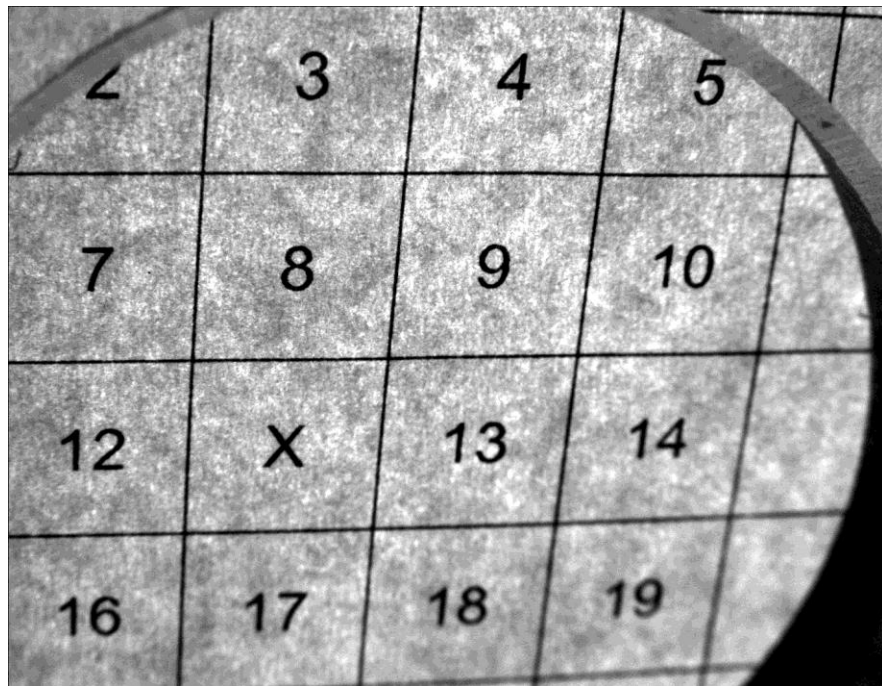
Fig. 17 Camera 2 capture of the Grid Pattern

The radial distortion in the projector is observed by projecting a grid pattern onto a flat surface and capturing the pattern with the cameras. The projected grid pattern captured by the center camera was barrel distorted as shown in Figure 18.
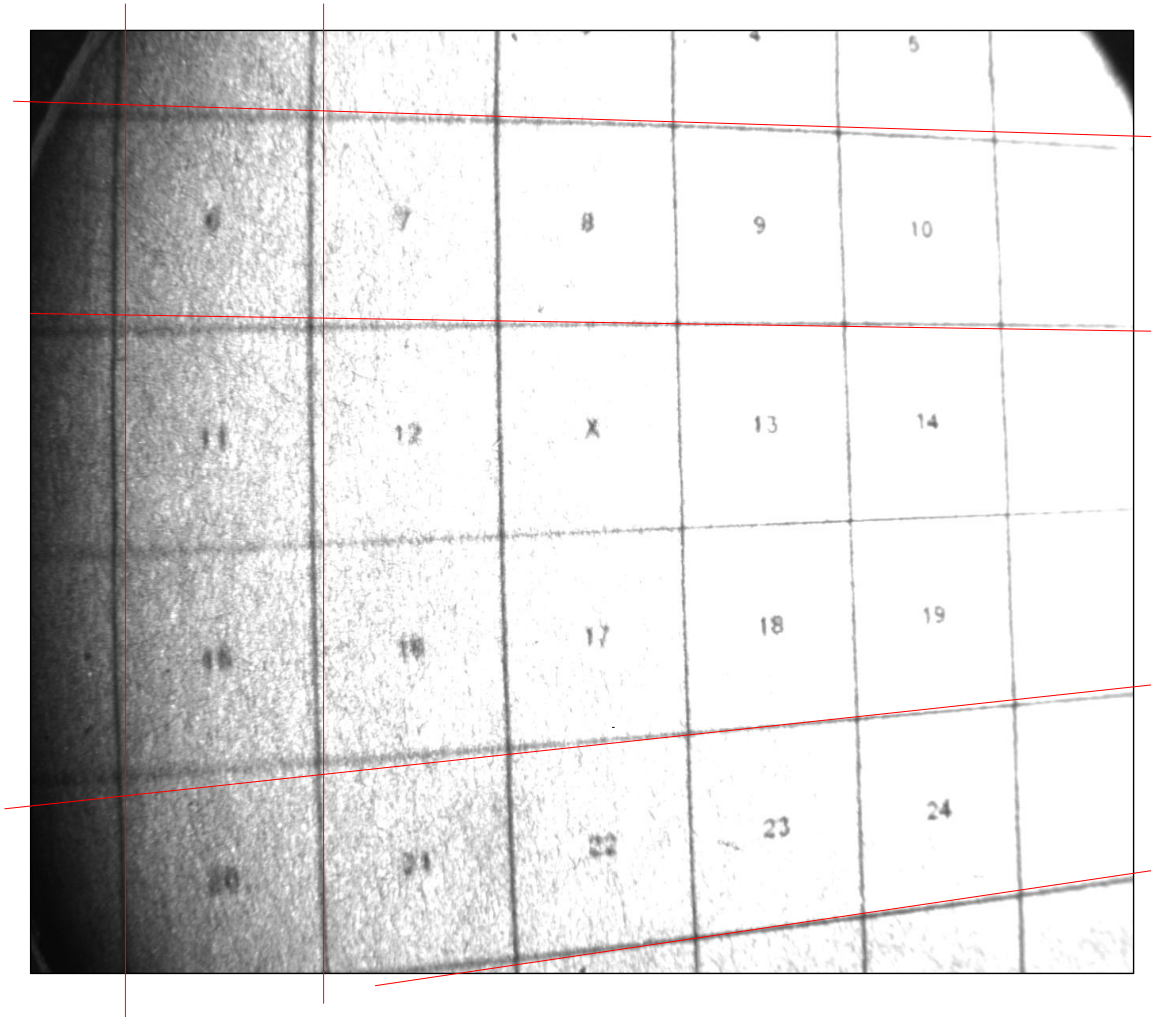
Fig. 18 Image from Projector and Center Camera showing Radial Distortion

Methodology for correcting Radial Distortion

The first step in correcting radial distortion is to determine the optical center. The second step involves the estimation of the radial distortion parameter [41].

i. *Determination of the optical center:* Given a set of points, with camera coordinates $(x_{c,n}, y_{c,n})$ and projector coordinates $(x_{p,n}, y_{p,n})$ for the corresponding world coordinates $(x_{w,n}, y_{w,n}, z_{w,n})$ where $z_{w,n} = z_w$ for all *n*, the relation between the camera and the world coordinates is represented by

$$x_{c,n} = a_{x,0} x_{w,n} y_{w,n}^2 + a_{x,1} x_{w,n} y_{w,n} + a_{x,2} x_{w,n} + a_{x,3} y_{w,n}^2 + a_{x,4} y_{w,n} + a_{x,5} \tag{3.17}$$

$$y_{c,n} = a_{y,0}x_{w,n}^2 y_{w,n} + a_{y,1}x_{w,n}y_{w,n} + a_{y,2}y_{w,n} + a_{y,3}x_{w,n}^2 + a_{y,4}x_{w,n} + a_{y,5} \qquad (3.18)$$

The coefficients of the quadratic equations are expressed in vector form as

$$A_x = [a_{x,0} \quad a_{x,1} \quad a_{x,2} \quad a_{x,3} \quad a_{x,4} \quad a_{x,5}] \qquad (3.19)$$

$$A_y = [a_{y,0} \quad a_{y,1} \quad a_{y,2} \quad a_{y,3} \quad a_{y,4} \quad a_{y,5}] \qquad (3.20)$$

Least squares solution technique is used to solve for the coefficients given by equations

$$A_x = x_c Y_x^{\mathrm{T}} R_{xx}^{-1} \qquad (3.21)$$

$$A_y = y_c X_y^{\mathrm{T}} R_{yy}^{-1} \qquad (3.22)$$

where

$$Y_x = \begin{bmatrix} x_{w,0}y_{w,0}^2 & \cdots & x_{w,n}y_{w,n}^2 & \cdots & x_{w,N-1}y_{w,N-1}^2 \\ x_{w,0}y_{w,0} & \cdots & x_{w,n}y_{w,n} & \cdots & x_{w,N-1}y_{w,N-1} \\ x_{w,0} & \cdots & x_{w,n} & \cdots & x_{w,N-1} \\ y_{w,0}^2 & \cdots & y_{w,n}^2 & \cdots & y_{w,N-1}^2 \\ y_{w,0} & \cdots & y_{w,n} & \cdots & y_{w,N-1} \\ 1 & \cdots & 1 & \cdots & 1 \end{bmatrix}, \qquad (3.23)$$

$$X_y = \begin{bmatrix} x_{w,0}^2 y_{w,0} & \cdots & x_{w,n}^2 y_{w,n} & \cdots & x_{w,N-1}^2 y_{w,N-1} \\ x_{w,0}y_{w,0} & \cdots & x_{w,n}y_{w,n} & \cdots & x_{w,N-1}y_{w,N-1} \\ y_{w,0} & \cdots & y_{w,n} & \cdots & y_{w,N-1} \\ x_{w,0}^2 & \cdots & x_{w,n}^2 & \cdots & x_{w,N-1}^2 \\ x_{w,0} & \cdots & x_{w,n} & \cdots & x_{w,N-1} \\ 1 & \cdots & 1 & \cdots & 1 \end{bmatrix} \qquad (3.24)$$

and $x_c = [x_{c,0} \dots x_{c,n} \dots x_{c,N-1}]^{\mathrm{T}}$, $y_c = [y_{c,0} \dots y_{c,n} \dots y_{c,N-1}]^{\mathrm{T}} \qquad (3.25)$

The relation between the camera and the world coordinates in reference to the camera optical center $(x_{c,c}, y_{c,c})$ and the world optical center $(x_{w,c}, y_{w,c})$ can be written as

$$(x_{c,n} - x_{c,c}) = \alpha(x_{w,n} - x_{w,c})(y_{w,n} - y_{c,c})^2, \qquad (3.26)$$

and $(y_{c,n} - y_{c,c}) = \beta(y_{w,n} - y_{w,c})(x_{w,n} - x_{c,c})^2 \qquad (3.27)$

Comparing equations (3.17) and (3.26) we get,

$$x_{w,c} = -\frac{a_{x,3}}{a_{x,0}} = -\frac{a_{x,4}}{a_{x,1}} = -\frac{a_{y,1}}{2a_{y,0}} = -\frac{2a_{y,2}}{a_{y,1}} = -\frac{a_{y,4}}{2a_{y,3}} \qquad (3.28)$$

Comparing equations (3.18) and (3.27) we get,

29

$$y_{w,c} = -\frac{a_{y,3}}{a_{y,0}} = -\frac{a_{y,4}}{a_{y,1}} = -\frac{a_{x,1}}{2a_{x,0}} = -\frac{2a_{x,2}}{a_{x,1}} = -\frac{a_{x,4}}{2a_{x,3}}$$ (3.29)

$$x_{w,c} = -\frac{a_{x,3}}{a_{x,0}} = -\frac{a_{x,4}}{a_{x,1}} = -\frac{1}{2}\left(\frac{a_{x,3}}{a_{x,0}} + \frac{a_{x,4}}{a_{x,1}}\right),$$ (3.30)

$$y_{w,c} = -\frac{a_{y,3}}{a_{y,0}} = -\frac{a_{y,4}}{a_{y,1}} = -\frac{1}{2}\left(\frac{a_{y,3}}{a_{y,0}} + \frac{a_{y,4}}{a_{y,1}}\right)$$ (3.31)

The camera optical center coordinates are given by

$$x_{c,c} = a_{x,2}x_{w,c} + a_{x,5}$$ (3.32)

$$y_{c,c} = a_{y,2}y_{w,c} + a_{y,5}$$ (3.33)

ii. *Estimation of the radial distortion parameter:* The mathematical equation for radial distortion correction is

$$r_{2,n} \approx r_{1,n} + \rho^3 r_{1,n}^3$$ (3.34)

where $r_{2,n}$ is the undistorted radius, $r_{1,n}$ is distorted radius and ρ is the radial distortion parameter.

The undistorted radius $r_{2,n}$ can be obtained most accurately from the world coordinates associated with that point given by

$$r_{2,n} = a_{r,0}r_{w,n} + a_{r,1}$$ (3.35)

where $r_{w,n} = \sqrt{(x_{w,n} - x_{w,c})^2 + (y_{w,n} - y_{w,c})^2}$

The coefficients in equation are solved using least squares solution such that

$$A_r = R_{rr}^{-1}R_w^{\mathrm{T}}r_c$$ (3.36)

where $A_r = \begin{bmatrix} a_{r,0} \\ a_{r,1} \end{bmatrix},$ (3.37)

$$r_c = [r_{c,0} \ \cdots \ r_{c,n} \ \cdots \ r_{c,N-1}]^{\mathrm{T}},$$ (3.38)

$$R_w = \begin{bmatrix} r_{w,0} & 1 \\ \cdot & \cdot \\ \cdot & \cdot \\ \cdot & \cdot \\ r_{w,n} & 1 \\ \cdot & \cdot \\ \cdot & \cdot \\ \cdot & \cdot \\ r_{w,N-1} & 1 \end{bmatrix} \tag{3.39}$$

and $R_{rr} = R_w^T R_w$ (3.40)

The undistorted radius is then calculated as

$r_2 = R_w A_r$ (3.41)

Knowing r_2 and $r_c^3 = [r_{c,0}^3 \quad \dots r_{c,n}^3 \quad \dots \quad r_{c,N-1}^3]^T$ in equation $r_2 = r_c + \rho^3 r_c^3$, the radial distortion parameter solution is

$$\rho^3 = \frac{(r_c^3)^T (r_2 - r_c)}{((r_c^3)^T r_c^3)} \tag{3.42}$$

Correction of Projector Radial Distortion

The barrel distortion in the projector as observed in figure 18 is corrected by first estimating the optical center of the projector and then determining the radial distortion coefficients. The resolution of the projector, monitor and the grid pattern are maintained equal. A grid pattern is projected onto a flat surface in the scan volume. The optical center of the projector is calculated assuming that the projector optical center usually lies at the bottom of the projector screen. After the optical center is determined, we manually vary the radial distortion parameter ρ and recalculate the image coordinates of the projected grid using the methodology explained in the second section of third chapter, until the barrel distorted lines in the grid pattern appear as straight lines. The optical center and the radial distortion parameter calculated from this method are used in the Multi fingerprint scanner program to radial correct the multi frequency patterns projected onto the 3D object in the scanning process.

The optical center of the projector was found to be $xp = 640$, $yp = 1000$ and the radial distortion parameter $\rho = -0.004$ with a projector resolution of 1280x1040 pixels.

Figures 19 and 20 show a grid pattern projected onto a plane surface before and after radial distortion correction respectively.
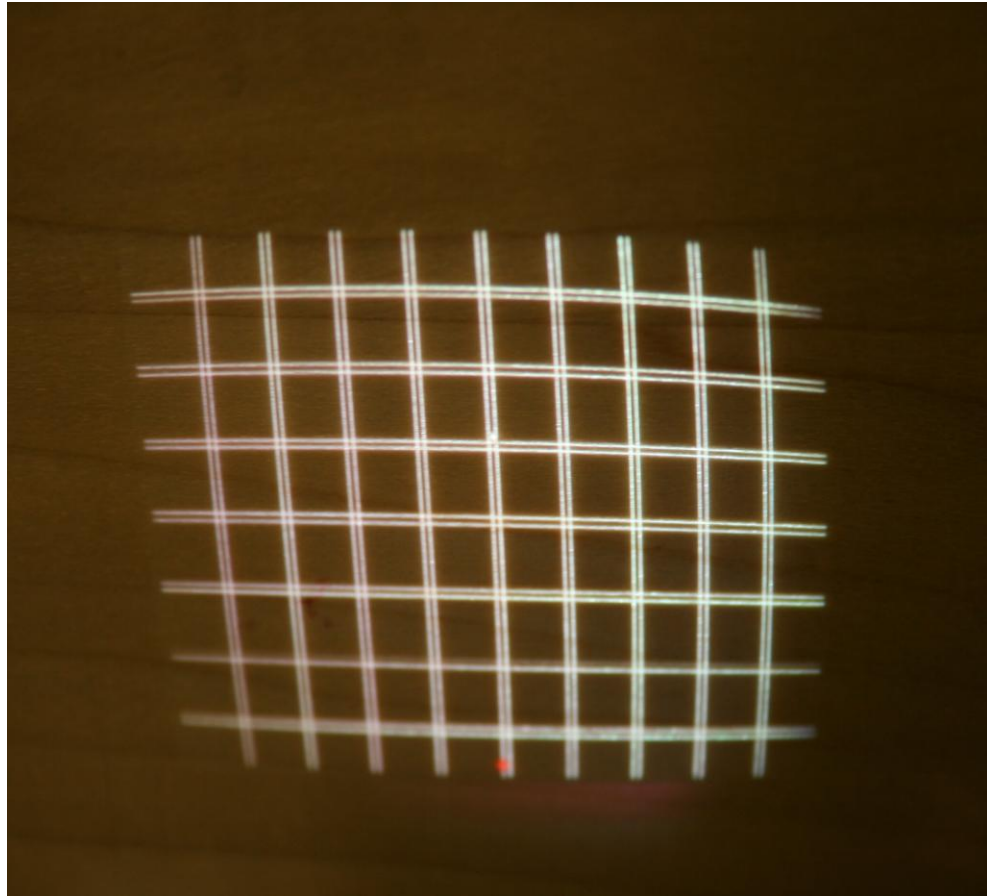

Fig. 19 Grid pattern from Projector before Radial Distortion Correction
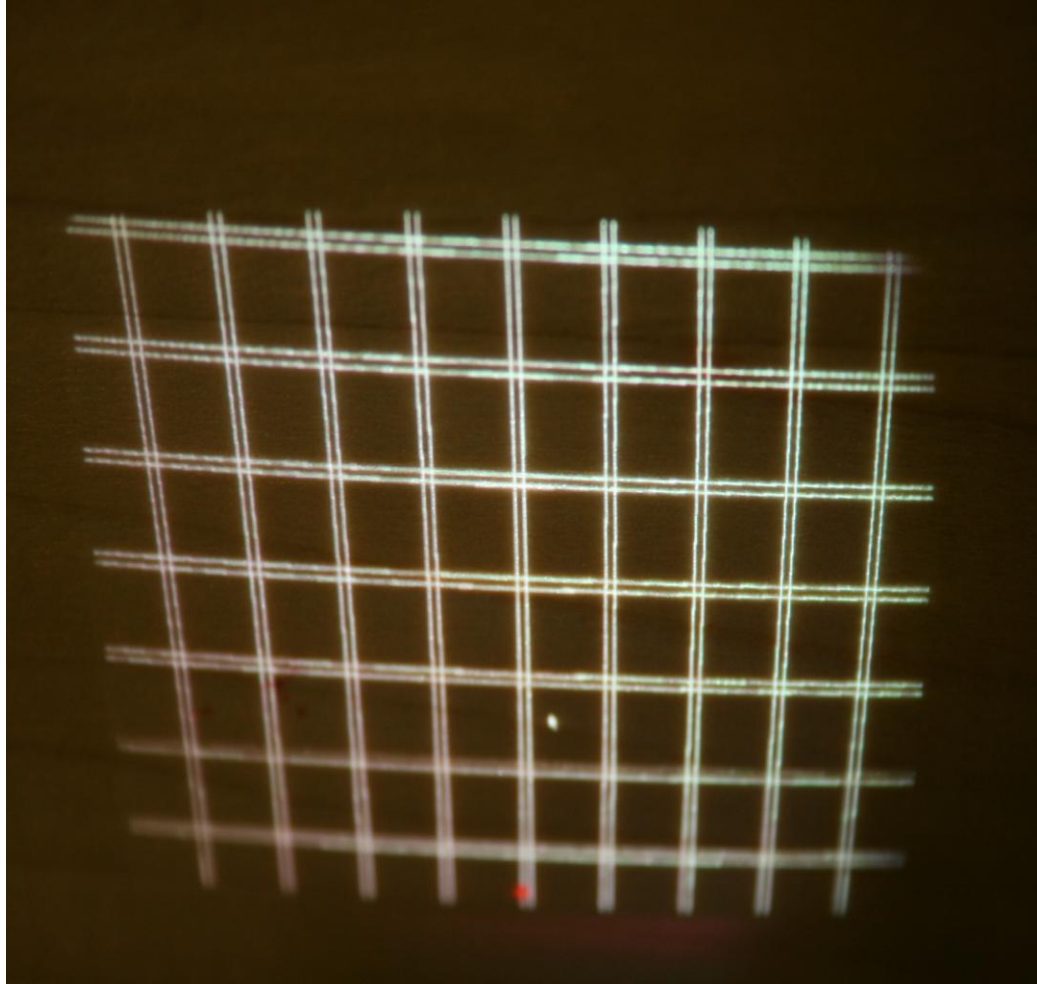
Fig. 20 Grid Pattern from Projector after Radial Distortion Correction

CHAPTER FOUR: MEASURING ACCURACY OF MERGED SCANS

In this chapter, the error in merging 3D scans from two cameras of the Scanner System is measured. In the first section of this chapter, the calibration data of the scanner system is analyzed. The distance between reconstructed world coordinates of reference calibration grid points from camera 0 and camera 1 is measured. In the second section of this chapter, the error in merged scan is measured by using projector space coordinates.

Multi-Camera 3D Fingerprint Scanner Calibration Data
Calibration is the foremost step in the process of 3D data acquisition using structured light illumination. Calibration establishes the geometry of the system and helps in accurate reconstruction of 3D data. It establishes a relation between world, camera and projector coordinates.

In this 3D fingerprint scanner system, a cylindrical shaped calibration grid was used which was marked with white lines spaced equally across the grid. The 3D world coordinates of the center of white lines are predetermined and are known as reference points $\left(X^w, Y^w, Z^w\right)$. During the process of calibration, multi frequency light patterns are projected onto the calibration grid and the images of the grid are captured by the cameras. The camera coordinates of the reference points are obtained manually from the images captured by the cameras. The projector coordinates of these points are obtained from the light patterns projected onto the calibration grid. A screenshot of the calibration software used to determine the camera and projector coordinates for the predetermined world coordinates is shown below in Figure 21. The figure shows the camera captured image, its cropped section and phase image used to determine y^p coordinate.

Fig. 21 Screenshot of Calibration Software used in determining camera coordinates and projector coordinates

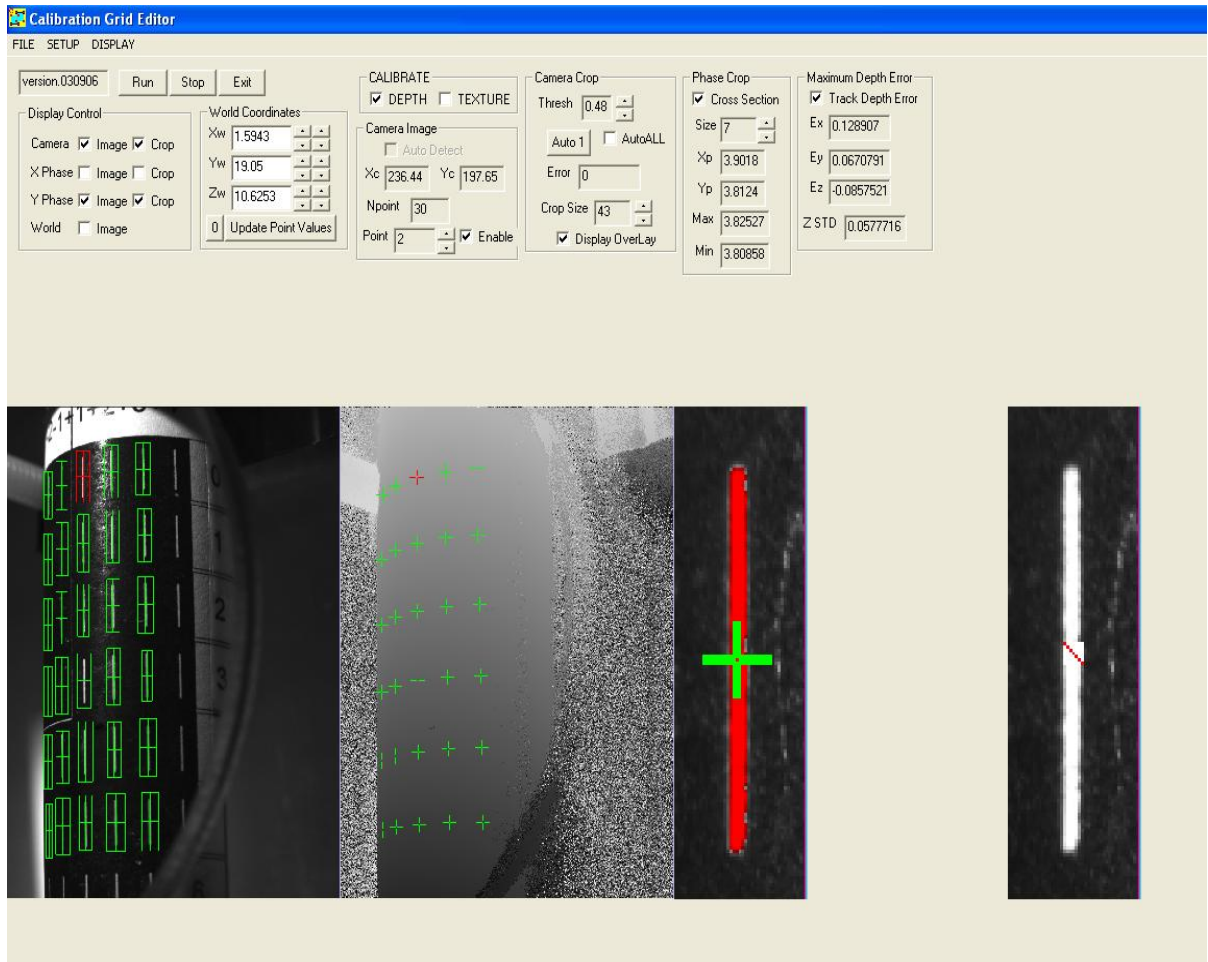The calibration data of Camera 0 and Camera 1 in the multi camera 3D fingerprint scanner system is shown in the tables 2 and 3 respectively.

Table 2 Calibration Data for Camera 0

Point	Xw	Yw	Zw	x^c	y^c	x^p	y^p	Error in Xw	Error in Yw	Error in Zw
1	7.2817	19.05	7.9003	457.778015	103.803001	2.931946	3.817384	0.032	-0.016	-0.062
2	4.6425	19.05	9.6894	556.598999	106.279999	3.222172	3.756811	0.051	-0.009	-0.083
3	1.5943	19.05	10.6253	646.330994	117.176003	3.550768	3.72173	-0.009	-0.002	-0.024
4	1.5943	19.05	10.6253	718.632996	136.988007	3.90728	3.721797	0.022	0.017	-0.032
5	4.6425	19.05	9.6894	766.109985	163.567993	4.247967	3.749548	0.021	-0.014	-0.017
6	7.2817	12.7	7.9003	458.313995	291.104004	2.927472	3.32594	-0.081	-0.017	0.071
7	4.6425	12.7	9.6894	558.549011	293.174988	3.203895	3.263858	-0.028	0	0.018
8	1.5943	12.7	10.6253	649.505005	303.962006	3.535354	3.225322	-0.046	-0.022	0.037
9	1.5943	12.7	10.6253	722.835022	320.950012	3.882589	3.221641	-0.046	-0.014	0.073
10	4.6425	12.7	9.6894	770.395996	342.369995	4.217545	3.257901	-0.009	0.042	0.033
11	7.2817	6.35	7.9003	459.112	482.149994	2.920648	2.86241	-0.05	0.072	0.04
12	4.6425	6.35	9.6894	560.625	485.325989	3.199576	2.790221	-0.034	0.017	0.038
13	1.5943	6.35	10.6253	652.284973	492.877014	3.514951	2.752456	-0.074	0.04	0.068
14	1.5943	6.35	10.6253	726.562988	510.056	3.864682	2.745343	0.008	-0.019	0.024
15	4.6425	6.35	9.6894	774.960999	528.575012	4.192835	2.77898	0.049	0.012	-0.002
16	7.2817	0	7.9003	460.093994	682.859009	2.917614	2.400905	-0.021	-0.014	0.019
17	4.6425	0	9.6894	562.875977	683.075012	3.189567	2.334804	0.052	0.025	-0.041
18	1.5943	0	10.6253	655.781006	691.690002	3.507895	2.287143	0.001	-0.048	0.013
19	1.5943	0	10.6253	730.088989	701.890991	3.845723	2.287898	0.052	0.019	-0.028
20	4.6425	0	9.6894	778.515015	718.833984	4.169693	2.312771	0.013	-0.039	0.007
21	7.2817	-6.35	7.9003	461.29599	886.422974	2.91555	1.959569	0.041	-0.038	-0.031
22	4.6425	-6.35	9.6894	564.869019	885.968994	3.189068	1.88896	0.071	-0.008	-0.058
23	1.5943	-6.35	10.6253	658.469971	891.070984	3.499391	1.846899	0.073	-0.012	-0.075
24	1.5943	-6.35	10.6253	733.192993	898.171997	3.833466	1.844356	0.074	0.044	-0.08
25	4.6425	-6.35	9.6894	781.820007	911.289001	4.154173	1.871176	0.055	-0.003	-0.076
26	7.2817	-12.7	7.9003	462.562012	1092.08997	2.916831	1.533432	0.039	0.002	-0.003
27	4.6425	-12.7	9.6894	566.767029	1090.80005	3.185789	1.4576	-0.013	0.027	0.037
28	1.5943	-12.7	10.6253	660.968994	1095.07996	3.495762	1.410535	-0.05	-0.016	0.036
29	1.5943	-12.7	10.6253	736.026001	1099.85999	3.82706	1.40324	-0.11	0.006	0.069
30	4.6425	-12.7	9.6894	784.372009	1107.70996	4.138371	1.433864	-0.146	0.004	0.053

Table 3 Calibration Data for Camera 1

Point	Xw	Yw	Zw	x^c	y^c	x^p	y^p	Error in Xw	Error in Yw	Error in Zw
1	-4.6425	19.049999	9.6894	126.558998	280.790009	3.22005	3.764492	0.04	0.02	-0.035
2	-1.5943	19.049999	10.625	166.906006	253.632004	3.54973	3.72252	0.021	-0.015	-0.025
3	1.5943	19.049999	10.625	234.320007	230.029007	3.90654	3.718139	-0.02	-0.004	-0.048
4	4.6425	19.049999	9.6894	322.609009	213.281006	4.24687	3.74455	-0.013	-0.004	-0.024
5	7.2817	19.049999	7.9003	422.667999	206.949005	4.53203	3.801705	-0.051	-0.019	-0.04
6	-4.6425	12.7	9.6894	125.169998	462.416992	3.2047	3.271078	0.026	0.029	0.027
7	-1.5943	12.7	10.625	166.768997	439.533997	3.53371	3.226707	0.032	-0.022	0.024
8	1.5943	12.7	10.625	234.690994	418.334015	3.88165	3.220274	0.033	-0.009	0.051
9	4.6425	12.7	9.6894	324.876007	402.306	4.21665	3.25323	0.037	0.044	0.036
10	7.2817	12.7	7.9003	426.459991	396.743011	4.49902	3.311335	0.026	0.015	0.032
11	-4.6425	6.35	9.6894	124.858002	650.099976	3.19849	2.791958	-0.008	-0.019	0.024
12	-1.5943	6.35	10.625	166.809998	629.16803	3.52057	2.74827	0.05	-0.015	0.071
13	1.5943	6.35	10.625	236.082001	611.927979	3.86429	2.745182	-0.015	0.002	0.013
14	4.6425	6.35	9.6894	327.104004	598.312988	4.19012	2.778242	-0.015	0.045	0
15	7.2817	6.35	7.9003	430.093994	593.215027	4.46777	2.833412	0.07	-0.007	0.082
16	-4.6425	0	9.6894	124.917999	839.530029	3.18937	2.336707	-0.082	0.019	-0.03
17	-1.5943	0	10.625	167.082001	825.125	3.50892	2.287133	-0.044	-0.045	0.009
18	1.5943	0	10.625	237.492004	809.455994	3.84615	2.286523	-0.07	0.021	-0.031
19	4.6425	0	9.6894	329.721008	799.645996	4.17178	2.313646	-0.01	-0.001	0.006
20	7.2817	0	7.9003	434.062012	795.575989	4.44387	2.378228	-0.041	-0.022	-0.039
21	-4.6425	-6.35	9.6894	125.570999	1035.31995	3.18815	1.888516	-0.095	-0.035	-0.055
22	-1.5943	-6.35	10.625	168.628998	1023.28003	3.49874	1.846105	-0.11	-0.018	-0.081
23	1.5943	-6.35	10.625	239.677002	1011.89002	3.83201	1.841451	-0.102	0.017	-0.085
24	4.6425	-6.35	9.6894	332.739014	1004.46002	4.15334	1.871816	-0.089	0.005	-0.086
25	7.2817	-6.35	7.9003	438.108002	1000.14002	4.42173	1.936107	-0.048	0	-0.053
26	-4.6425	-12.7	9.6894	127.459	1230.52002	3.18424	1.458364	0.086	0.048	0.04
27	-1.5943	-12.7	10.625	170.925995	1224.64002	3.4943	1.409762	0.096	0.01	0.044
28	1.5943	-12.7	10.625	242.688004	1218.07996	3.82579	1.40105	0.122	0.008	0.07
29	4.6425	-12.7	9.6894	336.468994	1212.89002	4.13685	1.433788	0.091	0.007	0.051
30	7.2817	-12.7	7.9003	442.371002	1210.03003	4.40404	1.50187	0.039	-0.007	0.026

The world, camera, projector coordinates and error in reconstruction of world coordinates of 30 reference points for each camera are shown in the tables above. There are a total of 24 points common to both cameras which have the same ideal world coordinates. Using the three sets of coordinates, the camera and projector transformation matrices for each camera are calculated using the least squares solution method. The 3D world coordinates of the reference points are reconstructed using the camera and projector transformation matrices. Ideally, the reconstructed world coordinates of all points common in both cameras should be equal. However, these coordinates from the two cameras are not the same due to various factors like calibration errors, lens distortions in cameras and projector and random noise in the system.

Let us denote the reconstructed world coordinates from camera 0 as $\left(X^{w1}, Y^{w1}, Z^{w1}\right)$ and camera 1 as $\left(X^{w2}, Y^{w2}, Z^{w2}\right)$. The squared distance between the reconstructed world coordinates is $(X^{w1} - X^{w2})^2 + (Y^{w1} - Y^{w2})^2 + (Z^{w1} - Z^{w2})^2$. This distance between

reconstructed world coordinates of the 24 reference points from the two cameras is plotted as a function of the ideal X^w and Y^w world coordinates of these points.

Figure 22 shows a 3D plot with X^w, Y^w on the x and y axis and distance between the reconstructed world coordinates on the z axis. Each colored line represents reference points with varying values of X^w for a constant Y^w value. From the figure we see that the difference in the reconstructed world coordinates from the two cameras is less than 0.05 mm with a majority of the points having an error less than 0.02 mm.
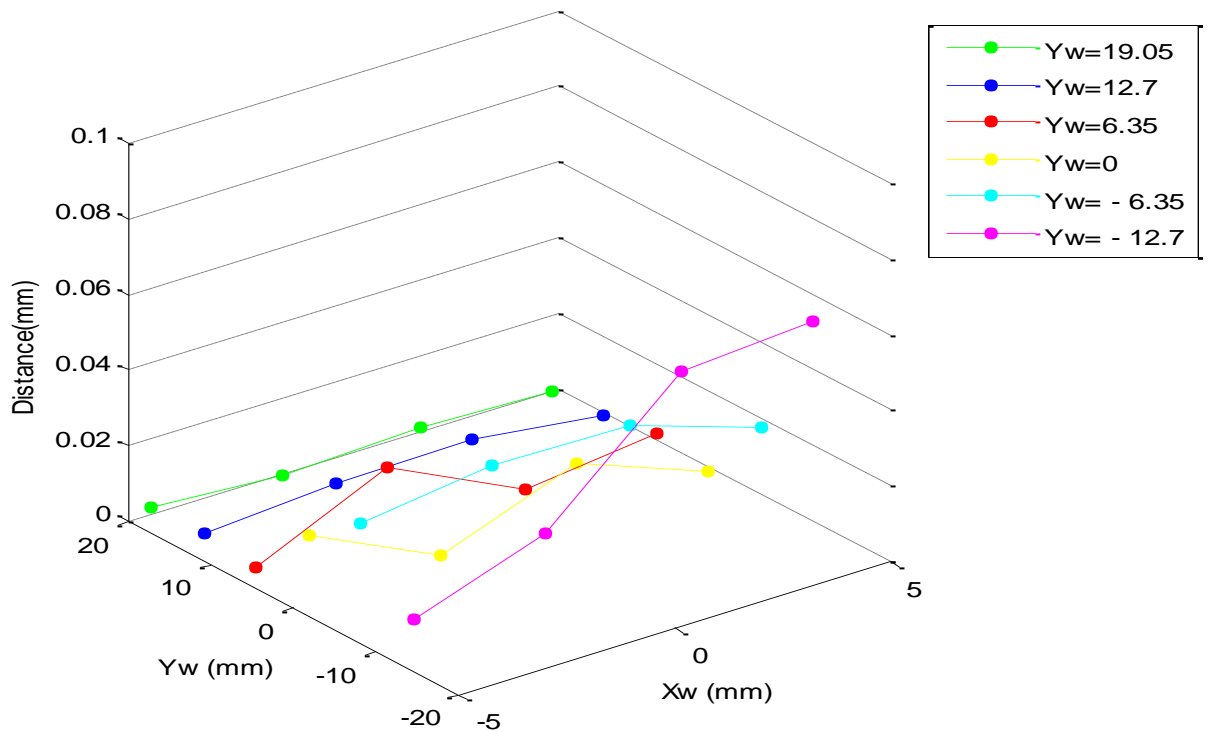

Fig. 22 Distance between the reconstructed world coordinates from Camera 0 and Camera 1 for the 24 reference points of the calibration grid

Merging in Projector Space

The 3D fingerprint scanner system uses three cameras placed at different angles with respect to the finger to capture 3D scans of the finger from different views. The 3D scans obtained from each camera have an overlapping section with the scans from other cameras. By merging scans obtained from all the cameras, a nail to nail view of the finger

with a higher resolution is obtained. However, due to distortions in scanner system and calibration errors, the 3D measurements (3D world coordinates) of the finger obtained from different cameras are not the same and hence the merged scans do not align automatically. The radial distortion correction of projector in the fingerprint scanner system reduced the error in merging to some extent but did not eliminate it completely. This error in merged scan is determined by finding the distance between world coordinates of corresponding points from the three cameras. The corresponding points between the three different cameras in a structured light system can be found based on the concept of projector space.

There are three coordinate systems involved in our fingerprint scanner system as shown in Figure 23. They are

    i)   3D World coordinate system $\left(X^w, Y^w, Z^w\right)$

    ii)   Camera coordinate system $\left(x^c, y^c\right)$

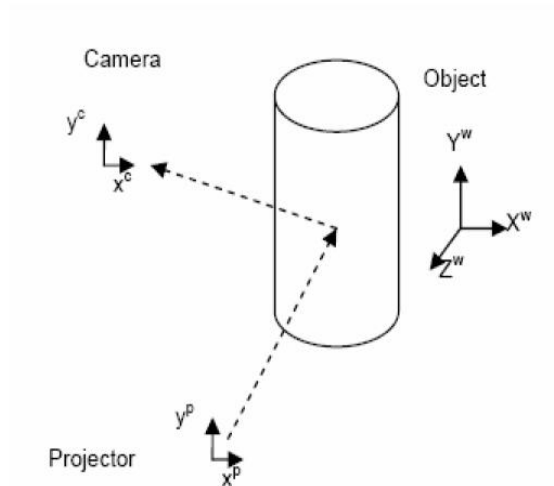   iii)   Projector coordinate system $\left(x^p, y^p\right)$

Fig. 23 Camera, Projector and World Coordinate Systems in a 3D Scanner System [42]

In the experimental setup of our multi camera fingerprint scanner system all the three cameras have the same projector space. Hence, ideally for a point in the 3D world coordinate system captured by the three cameras, the projector coordinates of this point

40

for all the three cameras should remain the same. Using this constraint, the corresponding points in the three cameras can be determined.

In this method, the two side cameras – camera 0 and camera 1 of the scanner system have been considered. The corresponding points from the two cameras should ideally have the same projector coordinates. But due to noise in the phase images captured by the cameras and distortions in the system, the projector coordinates are not exactly equal but very close to each other. Hence, for a point in camera 0, the point in camera 1 that has the nearest projector coordinates should be the corresponding point. So points in the two cameras that have the smallest projector coordinate distance are considered as corresponding points. After finding the corresponding points in both the cameras, the world coordinate distance between these points is calculated. This gives us a measure of the error in merging. If the world coordinate distance between corresponding points is very small, then the error in merged 3D scans from both the cameras is very small.

Methodology to find error in Merging of Scans from Two Cameras

i. A 3D object like calibration grid or finger is scanned in both the vertical (y^p) and horizontal (x^p) directions in the projector space. The phase information or projector coordinates of the 3D scan are stored in XP.byt and YP.byt files. The 3D scans obtained using the phase measuring profilometry (PMP) technique are stored in mat5 format. Mat5 format consists of 5 files - C.bmp (albedo image), I.bmp (intensity image), X. byt, Y. byt and Z. byt (x,y,z world coordinates) of the 3D scan.

ii. The 3D scan from camera 0 is considered as the parent scan and the scan from camera 1 as the child scan. The overlapping sections or the common area between the parent and child scans are determined.

iii. For every point in the overlapping section of the parent scan, we find the projector coordinate distance to all the points in the child scan.

iv. The point in the child scan that has the smallest projector coordinate distance to a point in the parent scan is considered as its corresponding point.

v. The mat5 indices of the corresponding point in the child scan for every point in the parent scan are stored in a mapping matrix.

vi. The mat5 indices can be used to determine the world coordinates of the corresponding points from the two cameras.

vii. The error in merging is given by the distance between the world coordinates of all the corresponding points in the overlapping section.

viii. For the 3D scans from the parent and child scans to align or merge exactly the distance between world coordinates of the corresponding points should be zero. If the distance is large then the error in merging is large.

Results of Merging in Projector Space

The calibration grid image captured by camera 0 and camera 1 is shown in figure 24(a) and 24 (b). To find the error in merging, we consider points in the calibration grid scan from camera 0 that are sampled every 20 pixels and marked in red. For every point marked in red in camera 0, the corresponding point in camera 1 is determined and marked in blue. The corresponding point in camera 1 is the point that has the nearest projector coordinates to the projector coordinates of the point in camera 0. The corresponding points are then merged in 3D world coordinate system as shown in figure 25. The error in merging of the corresponding points is calculated by finding the 3D world coordinate distance between them.
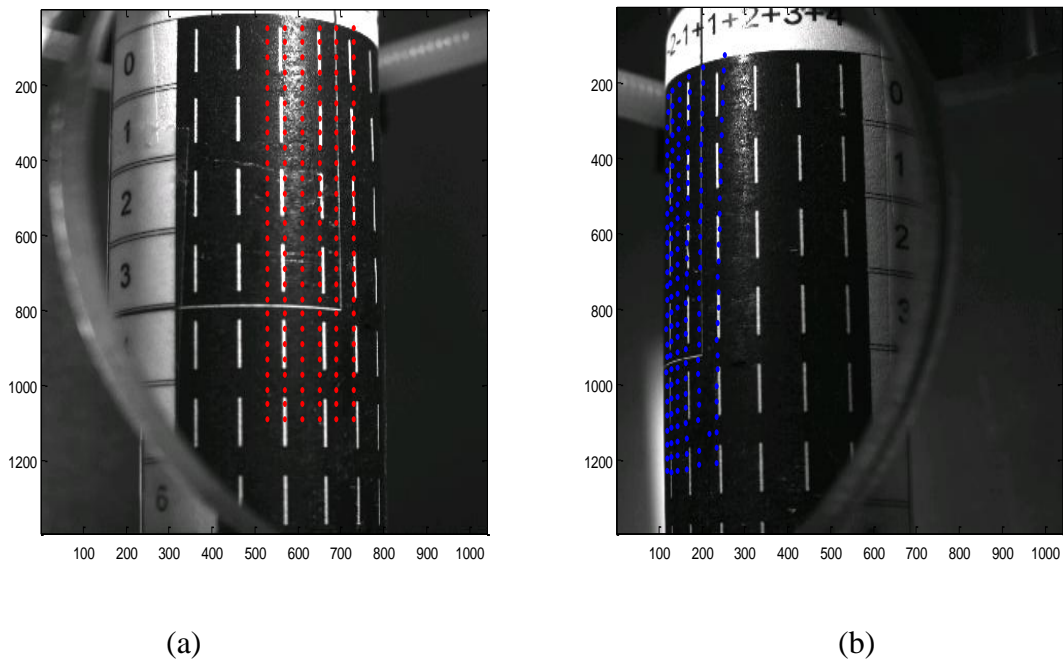

(a) (b)

Fig. 24 Calibration Grids from Camera 0 and Camera 1

42

Figures 24(a) and 24(b) show the calibration grids from camera 0 and camera 1 with the corresponding points marked in red and blue respectively which are determined using the projector space coordinates $\left(x^{p}, y^{p}\right)$.
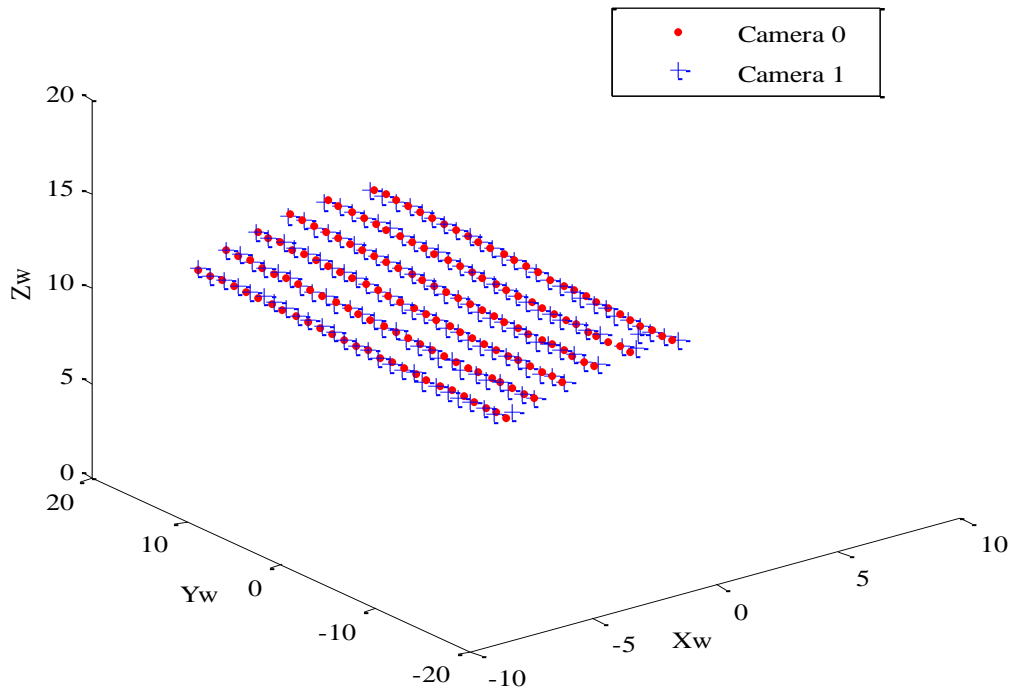

Fig. 25 Corresponding points from Camera 0 and Camera 1 merged in 3D world coordinate system.

The error in merging of corresponding points from Camera 0 and Camera 1 shown in Figure 25 is measured. 93% of the points have an error less than 0.05mm.

CHAPTER FIVE: EXPERIMENTAL RESULTS

In the first section of this chapter, the improvement in merging of 3D scans after correcting for radial distortion as described in Chapter 3 is presented. Merged 3D scans of various objects before and after distortion correction are presented to show the improvement. In the second section, we quantitatively measure the error or difference in reconstructed world coordinates from both the cameras using projector space coordinates. Finally the merged 3D scan of a fingerprint unraveled to a 2D rolled fingerprint is presented.

**Effect of Projector Radial Distortion Correction on Merging 3D scans**
This section presents the output 3D scans of different objects obtained by compensating for radial distortion in the projector of 3D fingerprint scanner system. The multi camera 3D fingerprint scanner system produces a 3D scan for each of the cameras. The output scans from all the cameras are merged to get a higher resolution, full 3D view of the object being scanned. The merged output is called super mat5.

The 3D scans of a calibration grid obtained from the two cameras are shown in Figures 26(a) and 26(b).The two calibration grids are merged to produce the super mat5 file as in Figure 26(c). A cropped section of the super mat5 image is shown in Figure 26(d).It is clearly seen from the super image that the two 3D scans do not overlap well.

Radial Distortion present in the projector of the fingerprint scanner system is compensated by the methodology explained in the third section of chapter three. The calibration grid 3D models from the two cameras after the distortion correction are shown in Figures 27(a) and Figure 27(b).The two 3D models are merged together to produce the super mat5 as in Figure 27(c) and a cropped section of the super mat5 is shown in Figure 27(d). The super mat5 produced after the distortion correction has clearly improved the merging or overlapping of the 3D models obtained from the two cameras.
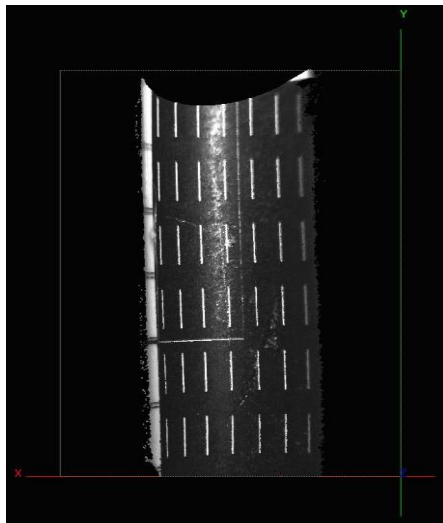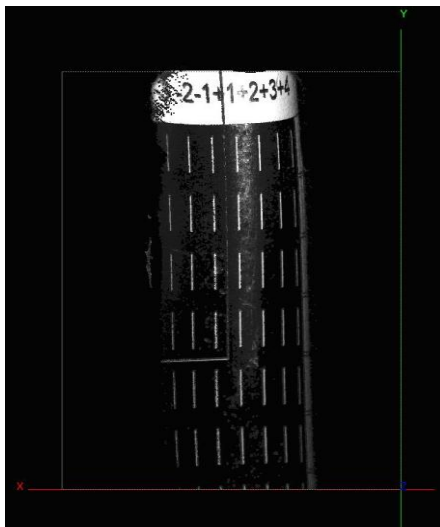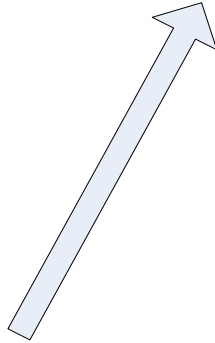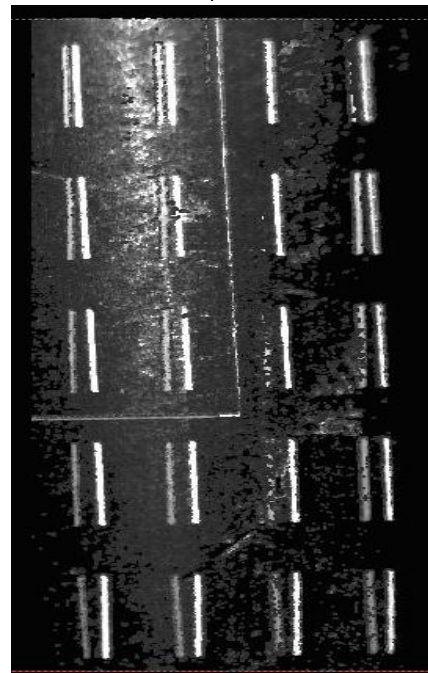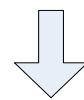
(a) Calibration Grid 3D Model from Camera 0
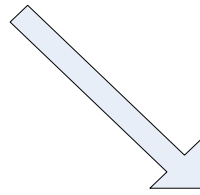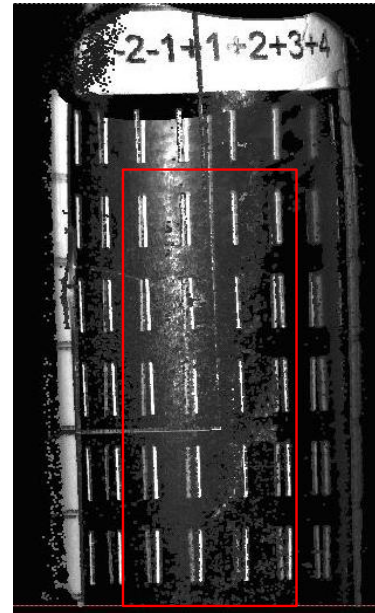
(b) Calibration Grid Super Mat5

Merging of 3D Models from Camera 0 and Camera 1

(c) Calibration Grid 3D Model from Camera 1

(d) Cropped Section of Calibration Grid Super Mat5

Fig. 26 Calibration Grid before Radial Distortion Correction

(a) Calibration Grid 3D Model from Camera 0
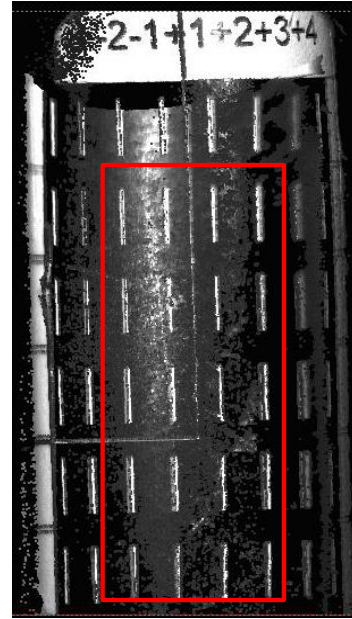
(b) Calibration Grid Super Mat5
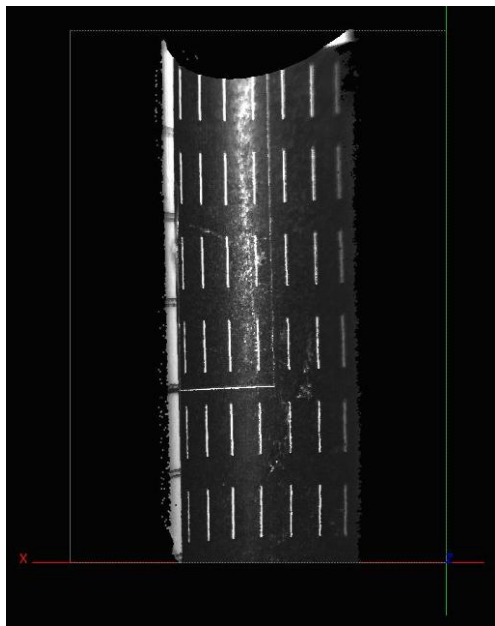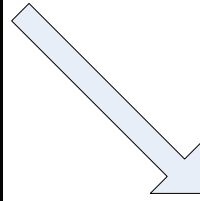
Merging of 3D Models from Camera 0 and Camera 1
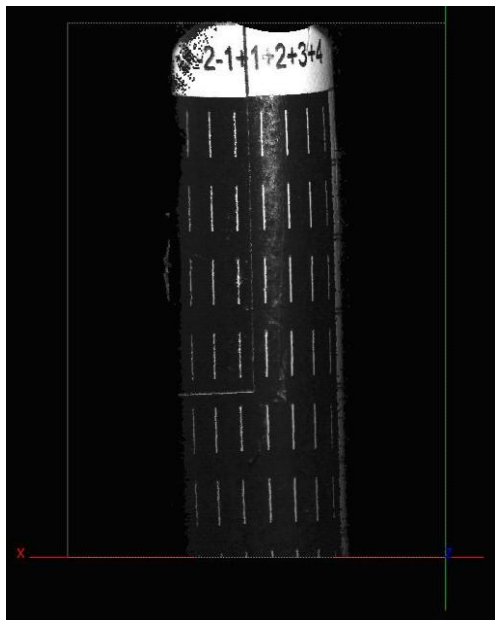
(c) Calibration Grid 3D Model from Camera 1
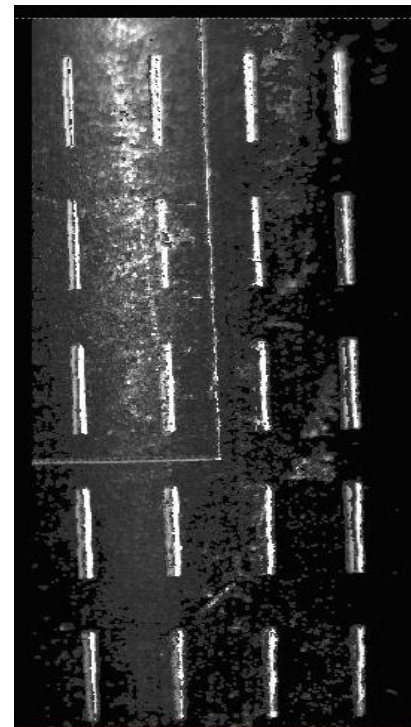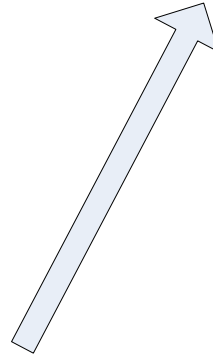
(d) Cropped Section of Calibration Grid Super Mat5

Fig. 27 Calibration Grid after Radial Distortion Correction

Super images of different objects before and after distortion correction are presented below.

(a) Super Mat5 of Coin

(b) Cropped Section of the Super Mat5 showing non overlapping regions from the two cameras

Fig. 28 Superimage of Coin before Radial Distortion Correction

(a) Super Mat5 of Coin

(b) Cropped Section of the Super Mat5 showing overlapping regions from the two cameras

Fig. 29 Superimage of Coin after Radial Distortion Correction

(a) 3D Model of Fingerprint from Camera 0

(b) 3D Model of Fingerprint from Camera 1

Fig. 30 3D Model of Fingerprint from Camera 0 and Camera 1

(c) Supermat5 of Fingerprint
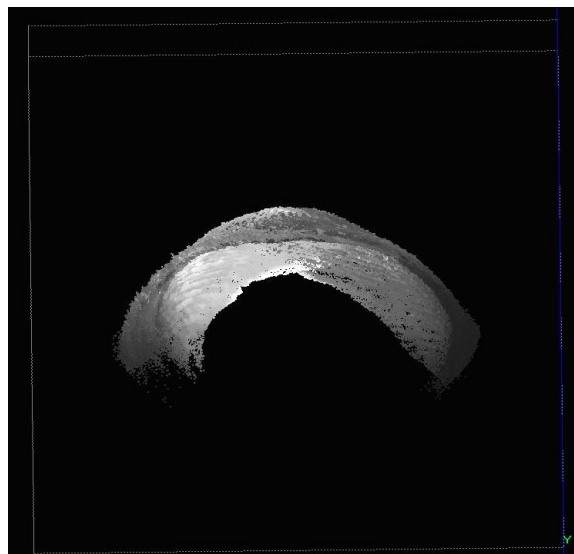
(d) View of Fingerprint Super Mat5

Fig. 31 Supermat 5 of Fingerprint

Measuring error in merged scans using projector coordinates obtained from both cameras

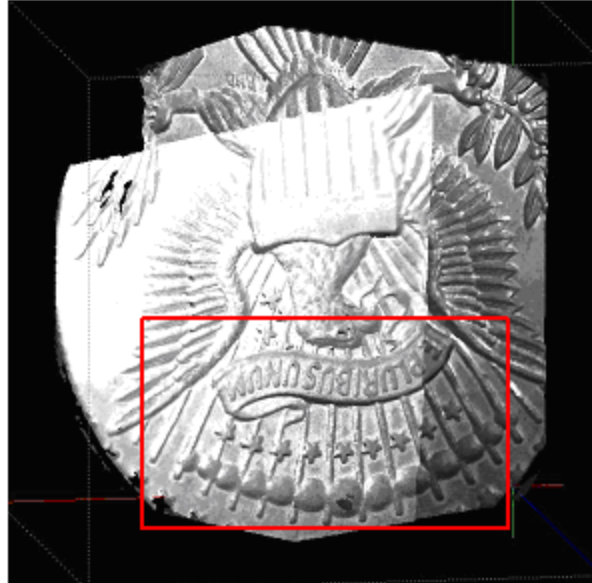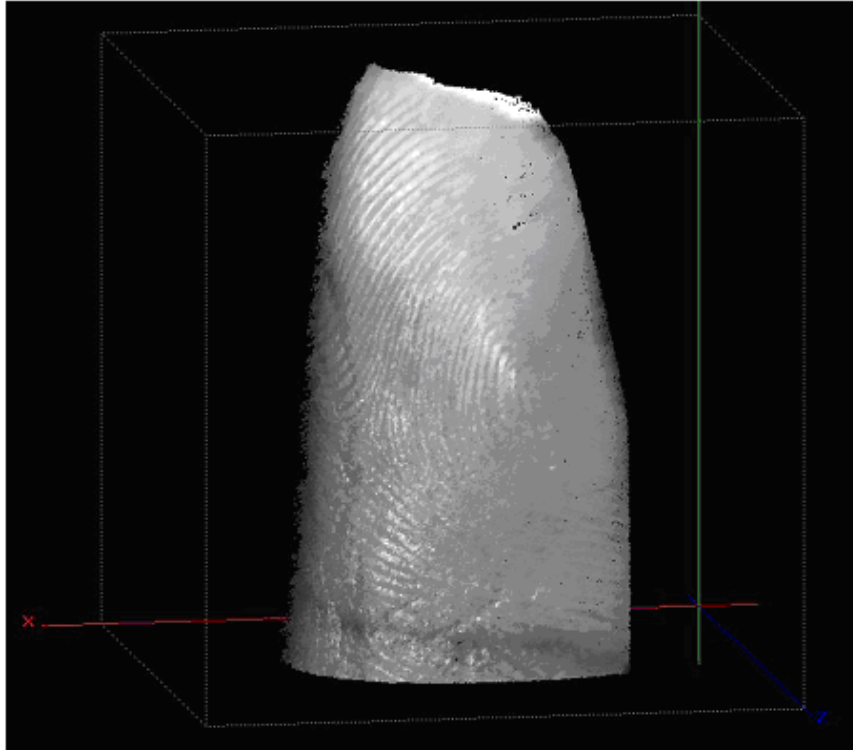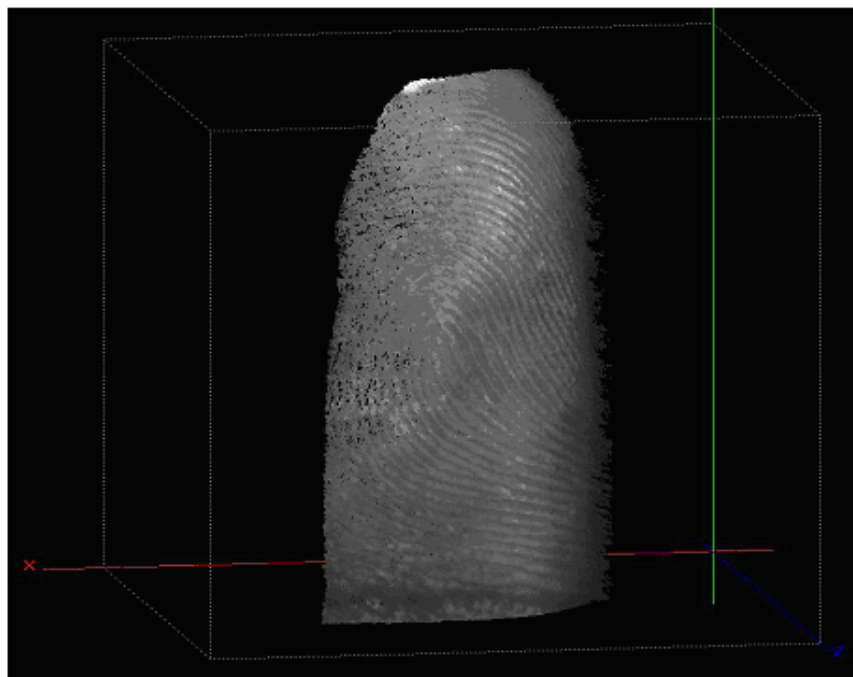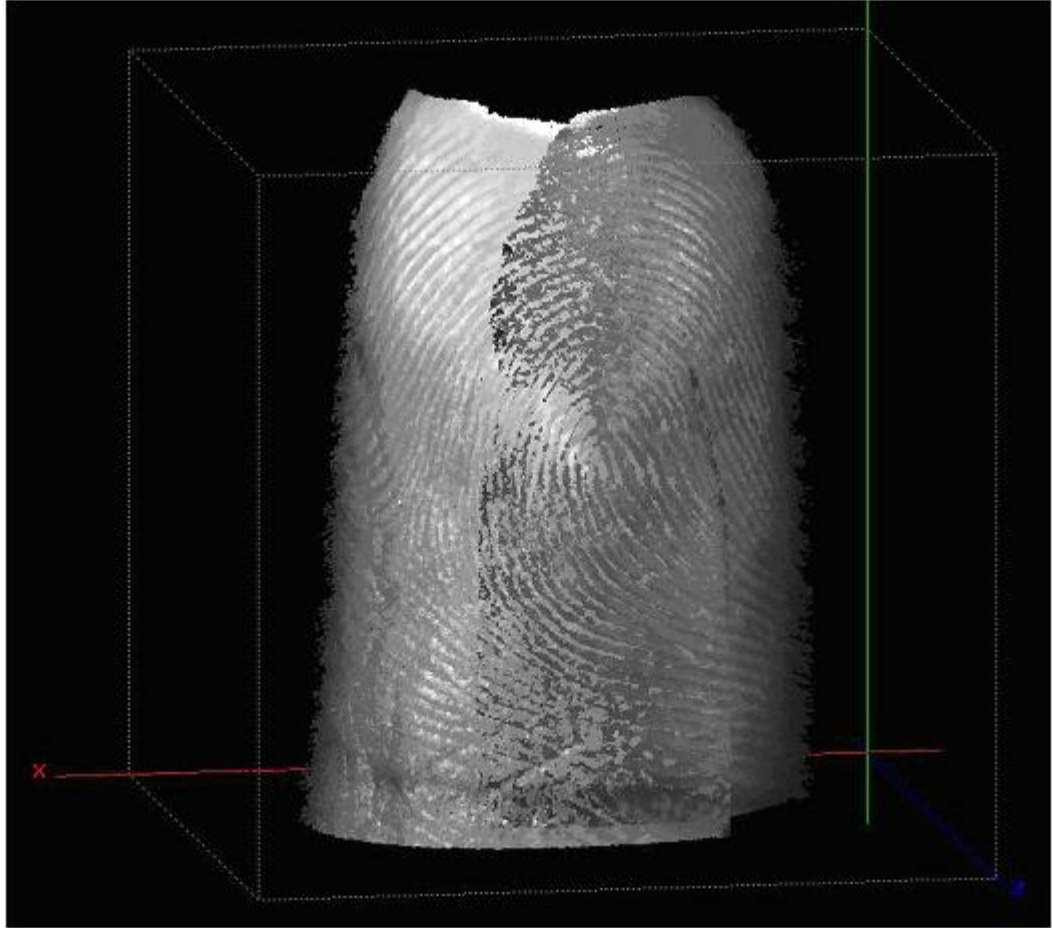The calibration grid images are captured by both cameras. To find the error in merging a set of points are sampled after every 20 pixels for the overlapping section of the two cameras and marked in red as shown in Figure 32(a). For every point marked red the corresponding point in camera 1 is the point that has nearest projector coordinates to the projector coordinates of the point marked in red. The corresponding points in camera 1 are marked in blue as shown in Figure 32(b). The world coordinates of these points are then plotted in 3D as shown in Figure 33. The world coordinate distance between these corresponding points gives the error in merging. From Figure 33, it can be seen that the error in merging of the calibration data is quite small. The error values are less than 0.5mm and majority of the points have an error less than or equal to .02mm.

Figure 34(a) and 34(b) show images of a fingerprint captured by both cameras. The corresponding points from camera 0 and camera 1 in the overlapping section of the cameras are determined and marked in red and blue respectively. The world coordinates are then plotted in 3D to show the amount of error or accuracy in merging. The error in merging for most of these points was found to be in the range of 0.05 mm to 0.01mm. In this way the accuracy of merging for different scans can be calculated.

Calibration Grid
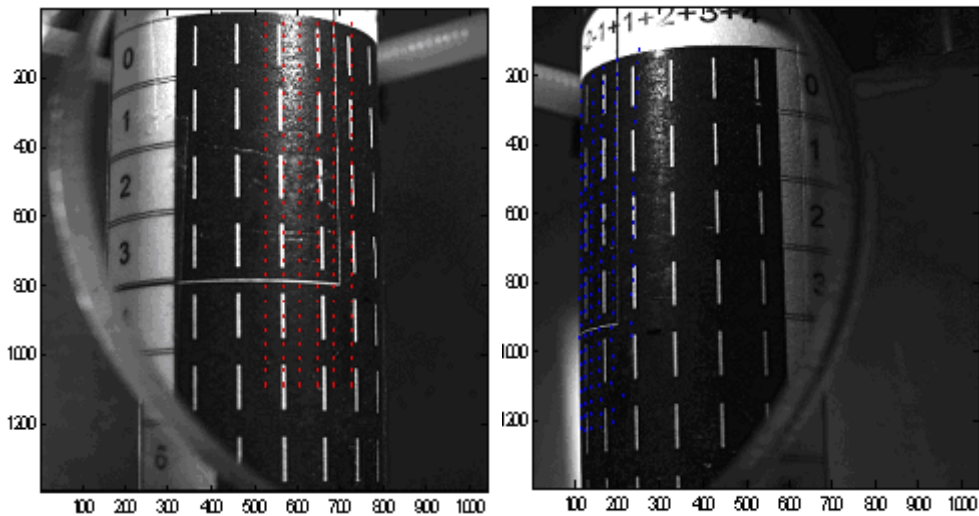
Fig. 32 Calibration Grid captured by Camera 0 and Camera 1

Figure 32 shows images of calibration grid captured by the two cameras with corresponding points in camera 0 and camera 1 marked in red and blue respectively
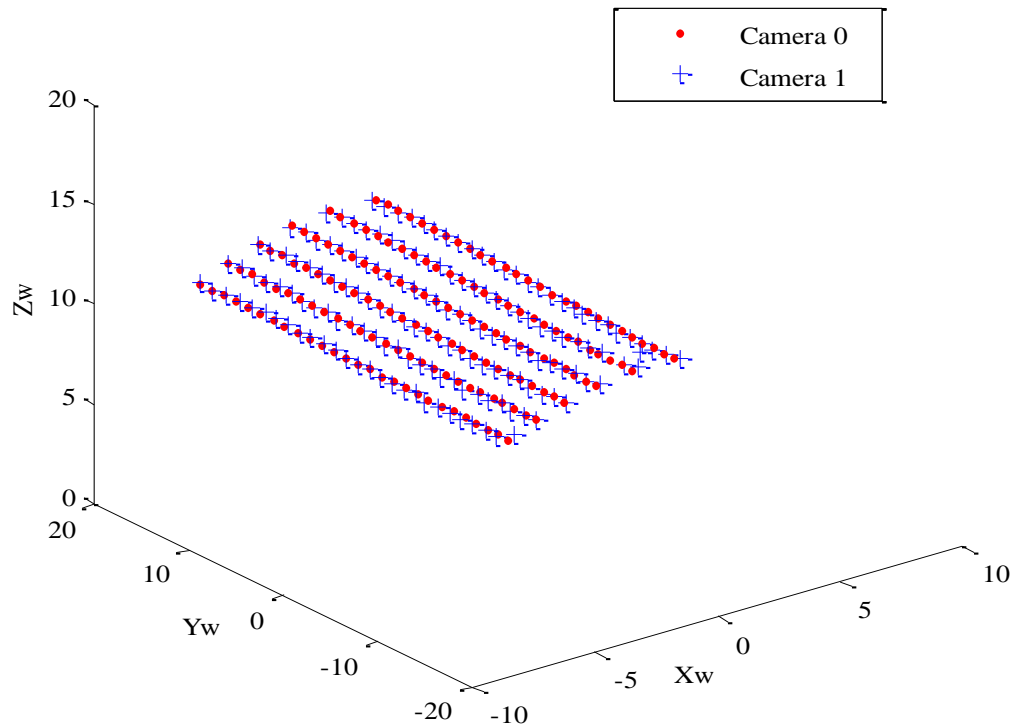
Fig. 33 World coordinates of the corresponding points from the two cameras plotted in 3D

This figure shows the amount of merging of corresponding points from the two cameras. The error in merging of corresponding points from Camera 0 and Camera 1 is measured. 93% of the points have an error less than 0.05mm.

Fingerprint

<table>
<tr><td>(a)</td><td>(b)</td></tr>
</table>
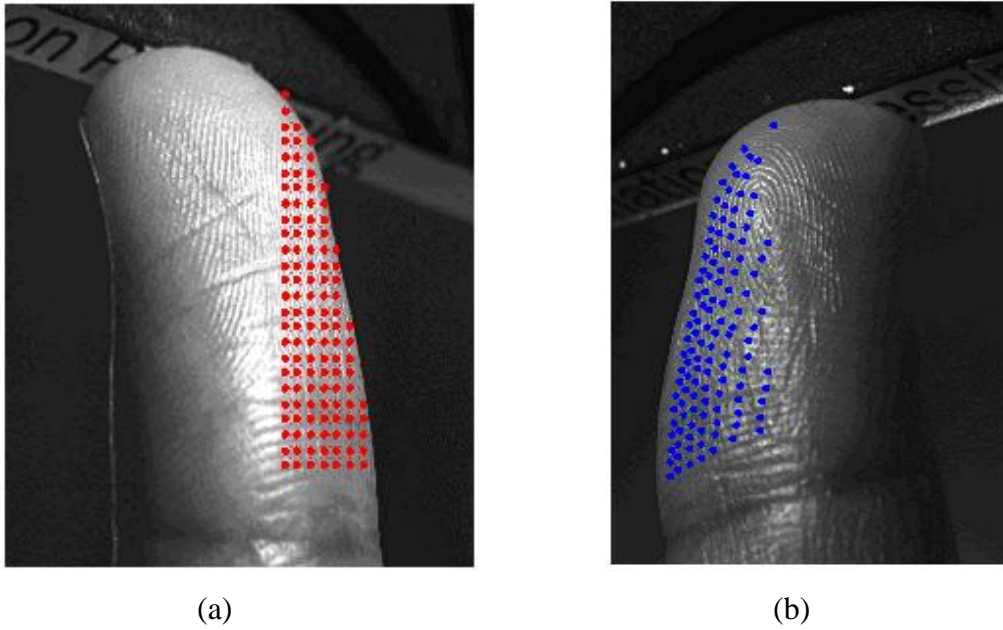
Fig. 34 Fingerprint images captured by Camera 0 and Camera 1

Figure 34(a) and Figure 34(b) show the fingerprint images captured by camera 0 and camera 1 with corresponding points marked in red and blue respectively.
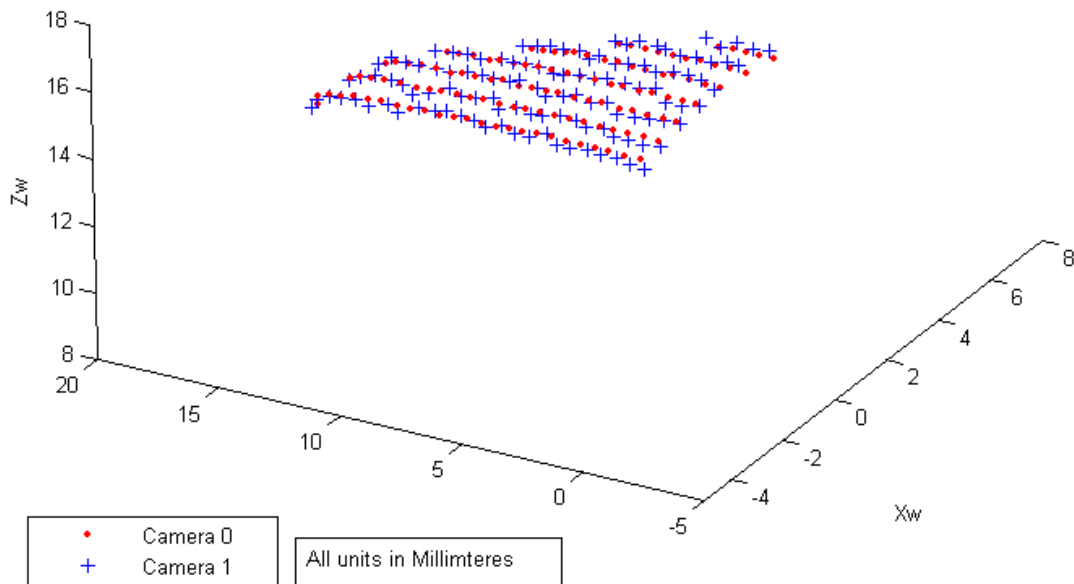
Fig. 35 World coordinates of corresponding points from Camera 0 and Camera 1 for fingerprint data plotted in 3D

53

3D Fingerprint Data Unraveled to 2D equivalent

The 3D fingerprint scans acquired by our scanner system need to be unraveled to 2D in order to be compatible with the rolled fingerprints that are currently used in government fingerprint database systems. The biggest challenge in using 3D fingerprint scans is its backward compatibility with legacy rolled images. Efforts are being made to effectively roll a 3D scan image into a 2D flat surface in the same way how inked rolled images are obtained.

The 3D data acquired by using our fingerprint scanner system is then unraveled into 2D images by Yongchang Wang, (Dept of Electrical Engineering, Center for Visualisation and Virtual Environment, University of Kentucky).The unraveling program uses a parametric model like a cylinder or sphere for unraveling the 3D to a 2D flat image. The unraveled images of 3D fingerprint data from camera 0 and camera 1 are shown in figure 36(a) and 36(b). The merged 2D image is shown in figure 36(c). From the unraveled images it can be seen that towards the side edges of the image the fingerprint features (ridges and valleys) are distorted. This can be seen even in the 3D fingerprint data. When these edges are merged the merged image shows some slightly distortions in the ridges and valleys. In order to view the alignment of ridges and valleys clearly in the merged image, binary images of the fingerprint images are shown in figures 37(a), 37(b) and 37(c).

<div align="center">

(a)

Unraveled 2D image from camera 0
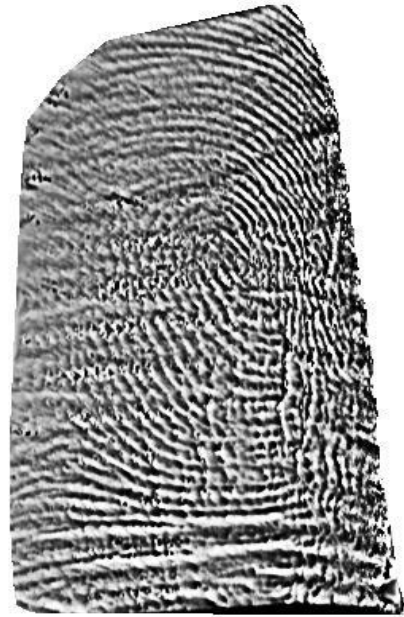
(b)

Unraveled 2D image from camera 1

</div>

<div align="center">

(c) Merged 2D image of Camera 0 and Camera 1 (Merging by Yongchang Wang)

Fig. 36 Unraveled 2D images from Camera 0, Camera 1 and Merged 2D Image

</div>

(a) Binary image of Camera0 image

(b) Binary image of Camera1

(c) Binary image of the merged 2D image

Fig. 37 Binary images from Camera0, Camera1 and Merged 2D Image

CHAPTER SIX: CONCLUSIONS AND FUTURE WORK

This thesis deals with the concepts of radial distortion correction, projector space merging and calibration accuracy for improving the merging of the 3D scans obtained from multiple cameras. First, the radial distortion in the projector is corrected. The effect of compensating radial distortion on merging is observed. Then using the projector coordinates from both cameras, the distance between corresponding points of the 3D scan from both the cameras are determined. The merged scans of various objects are shown to depict the results.

Conclusions

The radial distortion present in the projector of the scanner system is corrected. The new radially corrected patterns are projected onto the object to obtain 3D scans. The scans from the two cameras are merged together to produce a supermat5. It was observed that the merging of 3D scans improved after correcting for radial distortion of the projector. By compensating for radial distortion in the system, more accurate calibration is done and hence error in merging is reduced.

The phase information or projector coordinates of the scanner system are used to determine corresponding points from the two cameras. The object is scanned in both x and y directions to find corresponding points of the two cameras. The world coordinate distance between the corresponding points is calculated which gives the error in merging. A calibration grid and fingerprint scan showing the corresponding points and the distances between them are shown as examples. The error in the merging of these points was found to be a maximum of 0.05mm. If this error can be reduced to zero then the scans merge exactly.

Future Work

In this thesis, the error in merging was reduced significantly but not completely to zero. The system needs to be compensated for any other distortions that account for error in merging. This will give us a nail to nail fingerprint which can be unraveled to 2D accurately. The 2D unraveled images obtained from the 3D data and the rolled equivalents obtained using the ink technique or live scan technique should be made

compatible. This is crucial since the data acquired by the 3D fingerprint scanner can be used effectively only if it is rendered in the format used by the current fingerprint databases.

Visual C++ Function used for Radial Distortion Correction

```
// Code used in Main Program

double xc,yc,beta;
xc=640;yc=1000;beta=.004;
beta= -beta;beta=beta*beta*beta;
bmpvolumedistortioncorrect(bmpproj,pcols,prows,totpat,(double)xc,
(double)yc,(double)beta);

// Function used to correct radial distortion

void bmpvolumedistortioncorrect(BMPPIXEL *bmpvol,short Nx,short My,short
Pz,double xc,double yc,double beta)
{
        BMPPIXEL *bmpimage1,*bmpimage2;
        long *c2cm,*c2cn;
        long Nindex;
        short p;
        Nindex=(long)Nx*(long)My;
        bmpimage1=new BMPPIXEL [Nindex];
        bmpimage2=new BMPPIXEL [Nindex];
        c2cm=new long [Nindex];
        c2cn=new long [Nindex];
        // radial lut
        distortion2dlut(c2cn,c2cm,Nx,My,&beta,xc,yc,(float)xc,(float)yc);
        for(p=0;p<Pz;p++)
        {
                volume2bmp(bmpvol,bmpimage1,Nx,My,Pz,p);
                // radial correct
                distortionradial(bmpimage2,bmpimage1,c2cn,c2cm,Nx,My);

                bmp2volume(bmpvol,bmpimage2,Nx,My,Pz,p);
        }
        delete [Nindex] bmpimage1;
        delete [Nindex] bmpimage2;
        delete [Nindex] c2cm;
        delete [Nindex] c2cn;

}

// Function to create a 2D lut for distortion correction
```

```c
void distortion2dlut(long *c2cnlut,long *c2cmlut,short Nx,short My,double *Ar,double
xc2center,double yc2center,float xcenter,float ycenter)
{
        long m,n,index,m1,n1;
        double x,y,r1,r2,theta2,ftemp;
        for(m=0;m<My;m++)
        for(n=0;n<Nx;n++)
        {
                index=m*(long)Nx+n;
                // find r2
                r2=sqrt((((float)n-xc2center)*((float)n-
        xc2center)+((float)m-yc2center)*((float)m-yc2center));
                theta2=atan2((((float)m-yc2center),((float)n-xc2center));
                ftemp=(float)(r2*r2*r2);
                r1=r2+Ar[0]*ftemp;//+Ar[1]*ftemp*r2*r2;
                        x=r1*cos(theta2);
                        y=r1*sin(theta2);
                        m1=(long)(y+ycenter+0.5);
                        n1=(long)(x+xcenter+0.5);
                        if((m1>=0)&&(m1<My)&&(n1>=0)&&(n1<Nx))
                        {
                                c2cmlut[index]=m1;
                                c2cnlut[index]=n1;
                        }
                        else
                        {
                                c2cmlut[index]=-1;
                                c2cnlut[index]=-1;
                        }
                }
}

// Function to get the distortion corrected image

void distortionradial(BMPPIXEL *bmpimageout,BMPPIXEL *bmpimagein,long
*c2cn,long *c2cm,short Nx,short My)
{
        long index,index1,Nindex;
        Nindex=(long)Nx*(long)My;
        for(index=0;index<Nindex;index++)
        {
                if(c2cm[index]>=0)
                {
                        index1=c2cm[index]*(long)Nx+c2cn[index];
                        bmpimageout[index]=bmpimagein[index1];
                }
```

```
            else
bmpimageout[index].r=bmpimageout[index].g=bmpimageout[index].b=0;
        }
}
```

Matlab Code for finding Error in Merging of Scans from Camera 0 and Camera 1

```
clear all;
clc;

% fname1, fname2 are mat5 filenames for camera 0 and camera 1%

fnamec1=strcat(fname1,'C.bmp');
fnamec2=strcat(fname2,'C.bmp');
fnamei1=strcat(fname1,'I.bmp');
fnamei2=strcat(fname2,'I.bmp');
fnamex1=strcat(fname1,'X.byt');
fnamey1=strcat(fname1,'Y.byt');
fnamez1=strcat(fname1,'Z.byt');
fnamex2=strcat(fname2,'X.byt');
fnamey2=strcat(fname2,'Y.byt');
fnamez2=strcat(fname2,'Z.byt');
fnamexp1=strcat(fname1,'XP.byt');
fnameyp1=strcat(fname1,'YP.byt');
fnamexp2=strcat(fname2,'XP.byt');
fnameyp2=strcat(fname2,'YP.byt');

% reading from files %

c1=imread(fnamec1);
c2=imread(fnamec2);
[My,Nx,a]=size(c1);
i1=imread(fnamei1);
i2=imread(fnamei2);
fd=fopen(fnamex1);
xw1=fread(fd,'float');
fclose(fd);
fd=fopen(fnamey1);
yw1=fread(fd,'float');
fclose(fd);
fd=fopen(fnamez1);
zw1=fread(fd,'float');
fclose(fd);
fd=fopen(fnamex2);
xw2=fread(fd,'float');
```

```
fclose(fd);
fd=fopen(fnamey2);
yw2=fread(fd,'float');
fclose(fd);
fd=fopen(fnamez2);
zw2=fread(fd,'float');
fclose(fd);
fd=fopen(fnamexp1);
xp1=fread(fd,'float');
fclose(fd);
fd=fopen(fnameyp1);
yp1=fread(fd,'float');
fclose(fd);
fd=fopen(fnamexp2);
xp2=fread(fd,'float');
fclose(fd);
fd=fopen(fnameyp2);
yp2=fread(fd,'float');
fclose(fd);

% reshaping the matrices %

xw1=reshape(xw1,Nx,My)';
yw1=reshape(yw1,Nx,My)';
zw1=reshape(zw1,Nx,My)';
xw2=reshape(xw2,Nx,My)';
yw2=reshape(yw2,Nx,My)';
zw2=reshape(zw2,Nx,My)';
xp1=reshape(xp1,Nx,My)';
yp1=reshape(yp1,Nx,My)';
xp2=reshape(xp2,Nx,My)';
yp2=reshape(yp2,Nx,My)';

% initializing the variables %

p_m=zeros(My,Nx);
p_n=zeros(My,Nx);
p_dist=zeros(My,Nx);
p_world_dist=zeros(My,Nx);




% finding corresponding points of the two cameras %
```

```matlab
for m=row_i:5:row_f
   for n=col_i:5:col_f
      if i1(m,n) > 0
         % function for finding the closest point in projector space %
         [m2,n2,mindist]=closest_proj_point(m,n,xw1,yw1,zw1,c1,i1,xp1,yp1,xw2,yw2,z
         w2,c2,i2,xp2,yp2,Nx,My);
         p_m(m,n)=m2;
         p_n(m,n)=n2;
         p_dist(m,n)=mindist;
         % world coordinate distance between corresponding point %
         p_world_dist(m,n)=(xw1(m,n)-xw2(m2,n2))^2+(yw1(m,n)-
yw2(m2,n2))^2+(zw1(m,n)-zw2(m2,n2))^2;
         % marking the point in camera 0 in red %
         c1(m,n,1)=255;
         c1(m,n,2)=0;
         c1(m,n,3)=0;
         % marking the point in camera 1 in blue %
         c2(m2,n2,1)=0;
         c2(m2,n2,2)=255;
         c2(m2,n2,3)=0;
      end
   end
end

imwrite(c1,fnamec1);
imwrite(c2,fnamec2');


%%plotting the corresponding points in 3D space%%

for i=row_i:20:row_f
   for j=col_i:20:col_f
      if p_m(i,j) ~= 0
         figure(1),plot3(xw1(i,j),yw1(i,j),zw1(i,j),'r.');
         axis([-20,20,-20,20,0,20])
         hold on;
         plot3(xw2(p_m(i,j),p_n(i,j)),yw2(p_m(i,j),p_n(i,j)),zw2(p_m(i,j),p_n(i,j)),'b+');
         legend('Camera 0','Camera 1',2);
         hold on;
      end
   end
end


% Function for finding the nearest point in projector space in camera 1 for
```

a point in camera 0 or Finding corresponding points %

```
function [m2,n2,mindist]=closest_proj_point(m,n,xw1,yw1,zw1,c1,i1,xp1,yp1,xw2,yw2,
zw2,c2,i2,xp2,yp2,Nx,My)

xw=xw1(m,n);
yw=yw1(m,n);
zw=zw1(m,n);
xp=xp1(m,n);
yp=yp1(m,n);
k=0;
for i=1:My
   for j=1:Nx
      if i2(i,j) > 0
         d=(xp-xp2(i,j))^2+(yp-yp2(i,j))^2;
           if k = = 0
              mindist=d;
              m2=i;
              n2=j;
           elseif d < mindist
              mindist=d;
              m2=i;
              n2=j;
           end
           k=k+1;
      end
   end
end
```

REFERENCES

1. Dass, Sarat C.; Jain, Anil K.; *Fingerprint Based Recognition*; Technometrics, Volume 49, Number 3, August 2007 , pp. 262-276(15), American Statistical Association

2. http://www.ravirajtech.com/biometrics_fingerprint_technology.html#aaa

3. NSTC Subcommittee on Biometrics*; Fingerprint Recognition* available at http://biometrics.gov/Documents/FingerprintRec.pdf

4. Maltoni, Davide; Maio, Dario; Jain, Anil K.; Prabhakar, Salil; *Handbook of Fingerprint Recognition*; Jun. 2003, Springer, NY

5. Jain, Anil K.; Yi, Chen; Demirkus, M; Pores and Ridges: *High-Resolution Fingerprint Matching Using Level 3 Features*; Transactions on Pattern Analysis and Machine Intelligence, Volume 29, Issue 1, Jan. 2007, pp. 15 – 27

6. Keogh, E.; *An Overview of the Science of Fingerprints*; Anil Aggrawal's Internet Journal of Forensic Medicine and Toxicology, 2001; Vol. 2, No.1: Jan-Jun 2001

7. S. Prabhakar and A. K. Jain, "Fingerprint Matching", in *Automatic Fingerprint Recognition Systems*, N. Ratha and R. Bolle (eds.), Springer Verlag, New York, 2003.

8. Wilson, C. L.; Watson C. I.; Garris, M. D.; Hicklin, A.; *Studies of Fingerprint Matching Using the NIST Verfication Test Bed. (VTB)*; NIST Internal Report 7020, July 2003

9. Wilson, C. L.; Watson C. I.; Garris; *Matching Performance for the USVISIT IDENT System Using Flat Fingerprints*; NISTIR 7110, National Institute of Standards and Technology, May 2004

10. Stephen S. Wood; Charles L. Wilson; *Studies of Plain-to-Rolled Fingerprint Matching Using the NIST Algorithmic Test Bed (ATB)*; NISTIR 7112, National Institute of Standards & Technology

11. C.L. Wilson, *et al., Fingerprint Vendor Technology Evaluation 2003: Summary of Results and Analysis Report,* NISTIR 7123, National Institute of Standards and Technology, June 2004

12. Jin Chu Wu; Charles L. Wilson; *Nonparametric Analysis of Fingerprint Data*, NISTIR 7226, National Insitute of Standards and Technology

13. Jin Chu Wu; Charles L. Wilson; *Using Chebyshev's Inequality to determine sample size in Biometric evaluation of fingerprint data,* NISTIR 7273, National Insitute of Standards and Technology, Nov 2005

14. Geppy Parziale; Eva Diaz-Santana; *The Surround Imager^{TM}: a Multi-Camera Touchless Device to Acquire 3D Rolled-Equivalent Fingerprints*, TBS North America Inc.

15. Chen Y.; Parziale G.; Diaz-Santana E.; Jain, Anil K.; *3D Touchless Fingerprints: Compatibility with Legacy Rolled Images*, Proceedings of Biometric Symposium, Biometric Consortium Conference, Baltimore, MD, Sep 2006

16. R. A. Jarvis, "A perspective on range finding techniques for computer vision", *IEEE Trans. Pattern Anal. Mach. Intell.* 5(2), pp. 122-139, 1983

17. F. Blais, "A Review of 20 years of range sensor development", *Videometrics VII, Proceedings of SPIE-IS&T Electronic Imaging,* SPIE Vol. 5013, pp. 62-76, 2003

18. J. S. Massa, G. S. Buller, A. C. Walker, S. Cova, M. Umasuthan, and A. Wallace, "Time of flight optical ranging system based on time correlated single photon countin", *Appl. Opt.* 37(31), pp. 7298-7304, 1998

19. C. Guan, L. G. Hassebrook, and D. L. Lau, "Composite structured light pattern for three-dimensional video", *Optics Express,* 11(5), pp. 406-417, 2003

20. H. Takasaki, "Moire topography", *Appl. Opt.* 9**,** pp. 1467-1472, 1970.

21. S. D Cochran and G. Medioni, "3-D surface description from binocular stereo", *IEEE PAMI,* 14(10), pp. 981-994, 1992

22. J. Battle, E. Mouaddib, J. Salvi, "Recent progress in coded structured light as a technique to solve the correspondence problem: A survey ", *Pattern Recognition,*31(7), pp. 963-982, 1998

23. C. Guan, "Composite Pattern for Single Frame 3D Acquisition", *PhD Dissertation, University of Kentucky, Lexington,* USA, December 2004

24. P. M. Will and K. S. Pennington, Grid coding: a preprocessing technique for robot and machine vision, *Proc. Int. Joint Conf on Artificial Intelligence,* pp. 66-70, 1971

25. R. C. Daley and L. G. Hassebrook, "Channel capacity model of binary encoded structured lightstripe illumination", *Appl. Opt.,* 37(17), pp. 3689-3696, June 1998

26. V. Yalla and L. G. Hassebrook, "Very high resolution 3D surface scanning using multi frequency phase measuring profilometry" *SPIE Defense and Security, Spaceborne Sensors II,* Orlando, Florida, Vol. 5798-09, March 2005

27. Joaquim Salvi, Xavier Armangue, Joan Battle, "A comparative review of camera calibrating methods with accuracy evaluation", *Pattern Recognition,* 35, pp. 1617-1635, 2002

28. O. Faugeras and G. Toscani, "The Calibration problem for Stereo", *Proc. IEEE Conf. Computer Vision and Pattern Recognition,* pp. 15-20, June 1986

29. J. Weng, P. Cohen, M. Herniou, "Camera Calibration with distortion models and accuracy evaluation", *IEEE Trans. Pattern Anal. Mach. Intell.* 14, 965-980, 1992

30. R.Y. Tsai, "A versatile camera calibration technique for high-accuracy 3D machine vision metrology using off-the-shelf TV cameras and lenses", *IEEE Int. J. Robot. Automat. RA-3,* pp. 323-344, 1987

31. G. Q. Wei, S. De Ma, "Implicit and explicit camera calibration: Theory and experiments", *IEEE Trans. Pattern Anal. Mach. Intell.* 16, pp. 469-480, 1994

32. Z. Zhang, "A flexible new technique for camera calibration", *IEEE Trans. Pattern Anal. Mach. Intell.* 22(11), pp. 1330-1334, 2000

33. L. G. Hassebrook and C. Guan, "Distortion", *Encyclopedia of Optical Engineering*, edited by R. Diggers, published by Marcel Dekker, Inc., New York, pp. 428-434, 2003

34. Rahul Swaminathan and Shree K. Nayar, "Non metric calibration of wide angle lenses and poly cameras", *IEEE Trans. Pattern Anal. Mach. Intell.* Vol. 22, No. 10, October 2000

35. Janes Pers and Stanislav Kovacic, "Nonparametric, model-based radial lens distortion correction using tilted camera assumption", 2002

36. Richard Hartley and Sing Bing Kang, "Parameter-free radial distortion correction with center of distortion estimation", *IEEE Trans. Pattern Anal. Mach. Intell.* Vol. 29, No. 8, August 2007

37. L. Ma, Y. Q. Chen and K.L. Moore, "Analytical piecewise radial distortion model for precision camera calibration", *IEEE Proc.- Vis. Image Signal processing,* Vol. 153, No. 4, August 2006

38. De Xu, You Fu Li and Min Tan, "Method for calibrating cameras with large lens distortion", *Optical engineering,* 45(4), 043602 , April 2006

39. Thorsten Thormahlen and Hellward Broszio, "Automatic line based estimation of radial lens distortion", *Integrated Computer-Aided Engineering,* 12, pp. 177-190, 2005

40. Computer Vision: A Modern Approach. Prentice Hall, 2003

41. Laurence G. Hassebrook, Report on Spot Marker Radial Distortion Estimate, Mar 2007

42. Veera Ganesh Yalla, Multi Frequency Phase Measuring Profilometry, *Masters Thesis*, University of Kentucky, Lexington, 2004

VITA

Author's Name   Deepthi Boyanapally

Education   Bachelor of Technology in Electronics & Comm. Engineering
Jawaharlal Nehru Technological University
Hyderabad, INDIA
June 2005

Experience   Research Assistant
Center for Visualization and Virtual Environment
Department of Electrical Engineering
University of Kentucky
Lexington, KY USA

Birth Place   Warangal, India

Birth Date   Nov 11, 1983